

Resonant $dt\mu$ formation in condensed hydrogens

Andrzej Adamczak*

*Institute of Nuclear Physics, Polish Academy of Sciences,
Radzikowskiego 152, PL-31342 Kraków, Poland*

Mark P. Faifman†

*Russian Research Center Kurchatov Institute,
Kurchatov Square 1, RU-123182 Moscow, Russia*

(Dated: October 24, 2018)

Abstract

Resonant formation of the muonic molecule $dt\mu$ in $t\mu$ atom collision with condensed H/D/T targets is considered. A specific resonance correlation function, which is a generalization of the Van Hove single-particle correlation function, is introduced to calculate the resonant-formation rate in such targets. This function is derived in the case of a polycrystalline harmonic solid. Also is found a general asymptotic form of the resonance correlation function for high momentum transfers, valid for any solid or dense-fluid hydrogen-isotope target.

Numerical calculations of the rates are performed for solid molecular hydrogens at zero pressure, using the Debye model of an isotropic solid. It is shown that condensed-matter effects in resonant formation are strong, which explains some unexpected experimental results. In particular, the resonance profiles are affected by large zero-point vibrations of the hydrogen-isotope molecules bound in the considered crystals, even for high (~ 1 eV) collision energies. This is important for explanation of the time-of-flight measurements of the $dt\mu$ -formation rate, carried out at TRIUMF. The calculated mean values of the $dt\mu$ -formation rate in solid D/T targets, for fixed target temperatures and steady-state conditions, are in good agreement with the PSI and RIKEN-RAL experiments.

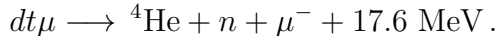
PACS numbers: 34.50.-s

*Electronic address: andrzej.adamczak@ifj.edu.pl

†Electronic address: mark@rogova.ru

I. INTRODUCTION

A theoretical study of resonant formation of the muonic molecular ion $dt\mu$ in condensed hydrogen-isotope targets is the main subject of this paper. Formation of $dt\mu$ is a key process of muon-catalyzed fusion (μ CF) in a D/T mixture, which attracted particular interest because one muon can catalyze more than 100 fusions [1–4] according to the reaction



Investigation of the μ CF cycle in various hydrogen-isotope targets is also important for studies of various phenomena in atomic, molecular, and nuclear physics (see reviews [5–7]).

Resonant $dt\mu$ formation is due to the presence of the loosely bound state of $dt\mu$ [1] with the rotational quantum number $J = 1$, the vibrational quantum number $v = 1$, and the binding energy $\varepsilon_{Jv=11} \approx -0.63$ eV. Theoretical methods for calculation of the resonant-formation rates were developed for many years (see e.g., Refs. [8–16]). These methods, taking into account resonant formation in $t\mu$ collision with one or few molecules, give good agreement with the experimental data for dilute gaseous targets. However, such theory is unable to explain various phenomena found in experiments with dense fluid and solid hydrogen-isotope targets. This concerns a nonlinear dependence of the formation rate on the target density [4, 17], puzzling temperature effects [18], and the resonance profiles determined by the time-of-flight experiments [19–22]. Therefore, it is necessary to consider the influence of many-body effects on muonic-molecule formation. In particular, various collective phenomena can significantly change this process, which one can expect knowing their role in resonant neutron absorption by nuclei bound in condensed matter [23, 24].

Condensed-matter effects in resonant neutron absorption can be expressed in terms of the single-particle correlation function [24], which has been introduced by Van Hove [25] for description of incoherent neutron scattering. This function depends on energy and momentum transfer to a target and its properties. It is possible to adapt this formalism to the case of resonant muonic-molecule formation.

First estimation of the $dt\mu$ -formation rate in solid molecular hydrogens was given by Fukushima [26]. He employed a correlation-function formalism, performed ab initio calculation of lattice dynamics to determine target properties, and demonstrated an important role of phonon processes in resonant $dt\mu$ formation. His calculation was limited to high target pressures (~ 10 kbar), where solid hydrogens are classical crystals. However, in μ CF experiments, only zero or low pressures ($\ll 10$ kbar) have been applied. As a result, the solid-hydrogen targets are quantum crystals with large amplitudes of zero-point vibrations of the molecules in the lattices and very different properties. Thus, a special approach is necessary to solve lattice dynamics [27, 28]. Owing to this fact and to a rough estimation of the transition-matrix elements for $dt\mu$ formation, the results of Ref. [26] are about five times greater than the rates determined in the experiments [2, 4]. Moreover, the temperature dependence of the calculated formation rate, for D_2 molecule bound in solid D/T, is opposite to what has been recently seen in the RIKEN-RAL experiment [18].

A theoretical method of calculating the resonant $dd\mu$ -formation rate, valid also for low-pressure solid hydrogens, has been presented in detail in Ref. [29]. The correlation function used for description of properties of solid polycrystalline D_2 has been derived for the Debye model of an isotropic solid. The model parameters, such as the Debye temperature and the lattice constants, has been taken from the available data including quantum-crystal effects [27, 28]. Since the resonances in $dd\mu$ formation on an free D_2 molecule are very

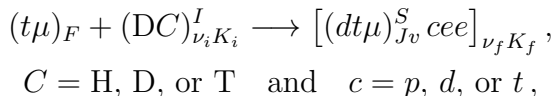
narrow, their profiles are well-described by the delta function. As a result, the corresponding formation rates in a solid are expressed in terms of the same incoherent correlation function that is employed for description of incoherent neutron scattering. The theoretical $dd\mu$ -formation rates lead to the time spectra of dd -fusion products that are in good agreement with the data taken at TRIUMF [30].

Below we present a method of calculation of the $dt\mu$ -resonant-formation rates in condensed hydrogens, for wide intervals of pressure and $t\mu$ collision energy. The profiles of $dt\mu$ resonances for a free-molecule are described by the Breit-Wigner function [9, 31]. In Ref. [24], such profiles have been taken into account for neutron or γ -ray resonant absorption by heavy nuclei. It has been assumed that the nuclear mass is not practically changed after absorption. As a result, a standard incoherent correlation function was sufficient for description of this process. In the case of muonic molecule formation in hydrogens, the mass of a target molecule increases greatly after muonic-atom absorption and creation of a small muonic-molecular ion. Therefore, we introduce a special resonance correlation function that includes this effect into the target dynamics. Only at lowest collision energies ($\lesssim 10$ meV), considered in Refs. [26, 29], an approximation that neglects this mass change can be applied since then resonant formation takes place practically in a rigid lattice. Such approach is valid for interpretation of experiments performed at lowest temperatures and well-described by steady-state kinetics. On the other hand, correct explanation of the time-of-flight experiments using energetic (~ 1 eV) beams of muonic atoms [20–22] require the knowledge of the formation rates at intermediate and higher energies.

In Sec. II, a brief description of resonant $dt\mu$ formation in an isolated hydrogen-isotope molecule is given. A method of calculation of the formation rates in condensed targets, using the energy-dependent transition-matrix elements obtained for a single molecule, is discussed in Sec. III. In particular, the formulas for the resonant-formation rates in harmonic polycrystalline hydrogens are derived. They can be applied to both $dt\mu$ and $dd\mu$ resonant formation. The results of numerical calculations for $dt\mu$ formation in low-pressure solid hydrogens are presented in Sec. IV. They have been obtained using a full set of the energy-dependent transition-matrix elements calculated for the free molecules HD, D₂, and DT. The $dt\mu$ formation rates for some typical solid targets are shown as functions of the $t\mu$ kinetic energy and target temperature. In particular, contributions from different resonances to the total formation rates and influence of the ortho-D₂ and para-D₂ concentration in a target on the formation rates are considered. A comparison of the calculated mean rates with some experimental results is performed.

II. RESONANT FORMATION IN A FREE MOLECULE

First we consider resonant formation of $dt\mu$ (the reasoning is analogical for the $dd\mu$ case) in the following reaction:



where DC is a free molecule in the initial rotational-vibrational state $(\nu_i K_i)$ with total nuclear spin **I**. This spin is taken into account for DC=D₂. The $t\mu$ atom has total spin **F** and center-of-mass (CMS) kinetic energy ε . The molecular complex $[(dt\mu)cee]$ is created in the rotational-vibrational state $(\nu_f K_f)$ and the molecular ion $dt\mu$, which plays the role

of a heavy nucleus of the complex, has total spin \mathbf{S} . This process takes place due to the presence of a loosely bound state of $dt\mu$ with rotational number $J = 1$ and vibrational number $v = 1$. The binding energy $|\varepsilon_{Jv=11}|$ released in the reaction above is transferred to rotational-vibrational degrees of freedom of the created molecular complex $[(dt\mu)cee]$. The resonance condition is fulfilled when ε takes a specific value ε_{if}^0 . This is so-called Vesman's mechanism of muonic-molecule formation, introduced in Ref. [8] for the $dd\mu$ case. In Fig. 1

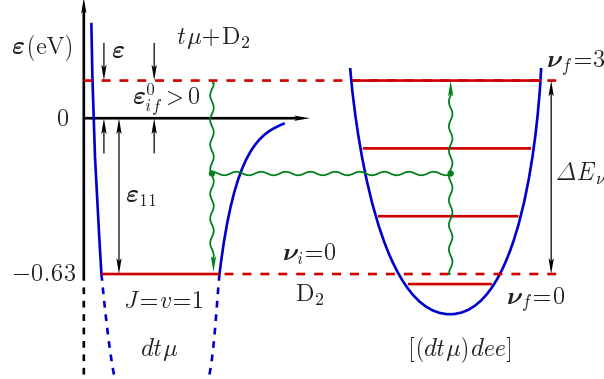


FIG. 1: Energy diagram for Vesman's mechanism of resonant $dt\mu$ formation in collision of a $t\mu$ atom with an isolated D_2 molecule.

is shown a scheme of energy balance for the $t\mu+D_2$ case. The formation rate $\lambda_{\nu_i K_i, \nu_f K_f}^{SF}$ depends on the elastic width $\Gamma_{\nu_f K_f, \nu_i K_i}^{SF}$ of $[(dt\mu)cee]$ decay [32, 33] through the channels:

$$[(dt\mu)_{Jv}^S dee]_{\nu_f K_f} \begin{cases} \xrightarrow{\Gamma_{\nu_f K_f, \nu_i K_i}^{SF}} (t\mu)_F + (DC)_{\nu_i K_i}^I \\ \xrightarrow{\lambda_f} \text{stabilization processes,} \end{cases}$$

where λ_f is the total rate of the stabilization processes, i.e., deexcitations of $dt\mu$ and nuclear fusion in $dt\mu$. The value of $\Gamma_{\nu_f K_f, \nu_i K_i}^{SF}$ is given (in atomic units $e = \hbar = m_e = 1$) by the equation

$$\Gamma_{\nu_f K_f, \nu_i K_i}^{SF} = 2\pi A_{if} \int \frac{d^3 k}{(2\pi)^3} |V_{if}(\varepsilon)|^2 \delta(\varepsilon_{if}^0 - \varepsilon), \quad (1)$$

The transition-matrix element is denoted by $V_{if}(\varepsilon)$ and the resonance energy ε_{if}^0 is defined in Ref. [13]. Factor A_{if} comes from averaging over initial projections and summing over final projections of the spins and angular momenta of the system. Vector \mathbf{k} is the momentum of relative motion of the $t\mu$ atom and the molecule DC, connected with kinetic energy ε by the relation

$$\varepsilon = k^2/(2\mathcal{M}),$$

in which \mathcal{M} denotes the reduced mass of the system. The general form of Eq. (1) follows from the Fano theory of resonant scattering [34]. Integration of this equation over \mathbf{k} leads to

$$\Gamma_{\nu_f K_f, \nu_i K_i}^{SF} = \frac{\mathcal{M} k_{if}^0}{\pi} A_{if} |V_{if}(\varepsilon_{if}^0)|^2, \quad k_{if}^0 = k(\varepsilon_{if}^0). \quad (2)$$

In the Vesman model, the resonance width is very small, so that the resonant-formation rate has the Dirac delta function profile

$$\lambda_{\nu_i K_i, \nu_f K_f}^{SF} = 2\pi N_{\text{mol}} B_{if} |V_{if}(\varepsilon)|^2 \delta(\varepsilon - \varepsilon_{if}^0). \quad (3)$$

where N_{mol} is the density of hydrogen-isotope molecules in the target. The coefficients A_{if} and B_{if} in Eqs. (1) and (3) are defined below

$$\begin{aligned} A_{if} &= W_{SF} \xi(K_i) \frac{2K_i + 1}{3(2K_f + 1)} q_d, \\ B_{if} &= W_{SF} \frac{2S + 1}{3(2F + 1)} q_d, \end{aligned} \quad (4)$$

where $W_{SF} = 1$ for $dt\mu$ and

$$W_{SF} = 3(2F + 1) \left\{ \begin{matrix} \frac{1}{2} & 1 & F \\ 1 & S & 1 \end{matrix} \right\}^2$$

in the $dd\mu$ case. The curly brackets stand here for the Wigner $3j$ symbol. For asymmetric molecules DC, function $\xi(K_i) = 1$ and in the case of D_2 we have

$$\xi(K_i) = \begin{cases} \frac{2}{3} & \text{for } K_i \text{ even} \\ \frac{1}{3} & \text{for } K_i \text{ odd.} \end{cases}$$

A value of factor q_d is connected with the number of deuterons in a considered system. When $dt\mu$ is created in $t\mu$ collision with an asymmetric molecule DC, $q_d = 1$, and if D_2 is a target molecule, $q_d = 2$. In the case of $dd\mu$ formation in an asymmetric DC system, factor $q_d = 2$. For $dd\mu$ formation in a D_2 target, one has $q_d = 4$. Coefficient B_{if} defined above differs from that introduced in Ref. [13] since we omit here the Boltzmann factor describing the population of the molecular rotational states in a gas target. We calculate the formation rate for a fixed initial rotational state. This rate is however averaged over total spin I of the target molecule. If the muonic atoms in the target have a steady kinetic-energy distribution $f(\varepsilon, T)$ at a fixed target temperature T , Eq. (3) can be additionally averaged over atomic translational motion, which gives a mean resonant rate $\tilde{\lambda}_{\nu_i K_i, \nu_f K_f}^{SF}(T)$.

Note that, for a given set of the initial and final quantum numbers, the resonance condition (cf. Fig. 1)

$$\varepsilon = \varepsilon_{if}^0 \quad (5)$$

can be fulfilled only when the variable $\varepsilon_{if}^0 = \varepsilon_{11} + \Delta E_\nu$ is positive.

In the case of resonant $dd\mu$ formation, the rates calculated using Eq. (3) agree very well with experiments [35, 36]. On the other hand, the assumption of the delta-function profile for $dt\mu$ resonances has led to inconsistency with experiments in gaseous D/T targets performed at low temperatures [3, 4, 37, 38]. The measured rates are much greater than the theoretical predictions based on the Vesman model. It has been pointed by Petrov [9] that the $dt\mu$ resonances should have broader Breit-Wigner profiles, owing to a finite lifetime of the complex. At low temperatures, this leads to significant contributions to the formation rates [39] from the subthreshold resonances $\varepsilon_{if}^0 < 0$. Thus, in a general free-molecule case, the resonance profile in Eq. (3) can be described by the Breit-Wigner function [9, 11]

$$\lambda_{\nu_i K_i, \nu_f K_f}^{SF} = N_{\text{mol}} B_{if} |V_{if}(\varepsilon)|^2 \frac{\Gamma_S}{(\varepsilon - \varepsilon_{if}^0)^2 + \frac{1}{4}\Gamma_S^2}, \quad (6)$$

where the total natural width Γ_S of the resonance is equal to a sum of the effective fusion rate λ_f and the total rate λ_{bck}^S of back decay of the complex

$$\Gamma_S = \lambda_f + \lambda_{\text{bck}}^S. \quad (7)$$

Equation (6) was employed in Refs. [16, 40] for calculation of $dt\mu$ formation rate in a dilute D_2 gas, which led to agreement with the experimental data [38]. In the limit $\Gamma_S \rightarrow 0$, the rate (6) tends to the Vesman form (3).

III. RESONANT FORMATION IN A CONDENSED TARGET

A. Method of calculation

When formation of a muonic molecule takes place in a dense target, it is necessary to take into account interactions of the impinging muonic atom with more than one molecule. In particular, energy transfer to many molecules is possible, which results in a quasisresonant character of the formation process. A quasisresonant mechanism of $dt\mu$ formation was first considered in Ref. [10], for triple collisions $t\mu + D_2 + D_2$, in order to explain a nonlinear density dependence of the $dt\mu$ formation rate. In this case, formation is possible even if the resonance condition (5) is not strictly fulfilled, because an energy excess in the $t\mu + D_2$ system is transferred to the second D_2 molecule. The three-body reactions and broadening of the resonance profiles were then discussed in Refs. [12, 15, 31, 39]. If a target is condensed, it is indispensable to take into account collective motions of target molecules in the process of resonant formation. In Fig. 2 is presented a scheme of quasisresonant $dt\mu$ formation

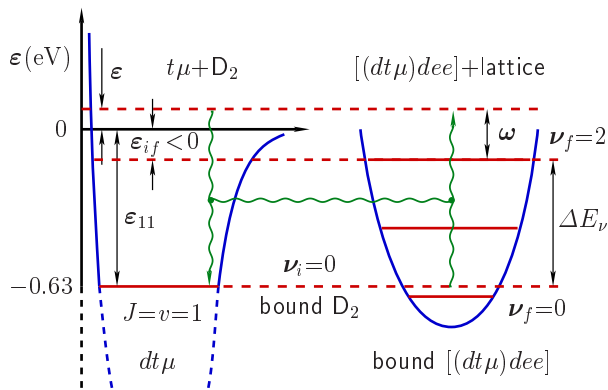


FIG. 2: Energy diagram for quasisresonant formation of $dt\mu$ in a D_2 molecule bound in a condensed target.

in $t\mu$ collision with a bulk condensed D_2 target. The energy balance, including energy transfer ω to the target, is shown for the subthreshold resonance corresponding to the transition $\nu_i = 0 \rightarrow \nu_f = 2$. Since the target molecule and the complex $[(dt\mu)dee]$ are bound, the corresponding resonance energy ε_{if} is different from the “free” resonant energy ε_{if}^0 , characterized by the same set of the quantum numbers.

Owing to a certain analogy between resonant absorption of neutrons and resonant formation of muonic hydrogen molecules, the methods developed in neutron physics can be

adapted for calculation of the rates of resonant $dd\mu$ and $dt\mu$ formation. Resonant neutron absorption and emission in condensed targets was first considered by Lamb [23]. His method was then generalized by Singwi and Sjölander [24], using the single-particle response function \mathcal{S}_i [25], and applied for description of resonant absorption and emission of γ ray and neutrons in condensed matter. In this Section are derived some expressions for the rate of muonic molecule formation in muonic atom collision with molecule DC, bound in a bulk hydrogen-isotope target.

A Hamiltonian \mathcal{H}_{tot} of the system, consisting of a $t\mu$ atom in the $1S$ state and a bulk condensed DC target, can be written down as follows

$$\begin{aligned} \mathcal{H}_{\text{tot}} = & \frac{1}{2M_{a\mu}} \nabla_{\mathbf{R}_{t\mu}}^2 + \mathcal{H}_{t\mu}(\mathbf{r}_1) + \mathcal{H}_{\text{DC}}(\boldsymbol{\varrho}_1) \\ & + V(\mathbf{r}_1, \boldsymbol{\varrho}_1, \boldsymbol{\varrho}_2) + \mathcal{H}, \end{aligned} \quad (8)$$

where $M_{a\mu}$ is the muonic atom mass and $\mathbf{R}_{t\mu}$ denotes the position of $t\mu$ center of mass in the coordinate frame connected with the target (see Fig. 3). Operator $\mathcal{H}_{t\mu}$ is the Hamiltonian

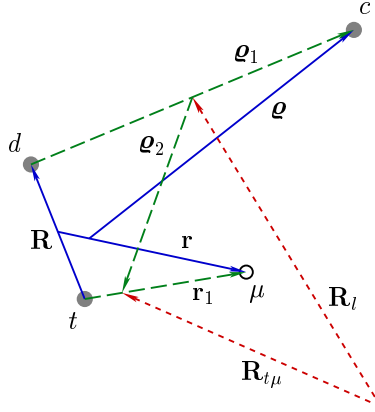


FIG. 3: System of coordinates used for calculation of the formation rate of the complex $[(dt\mu)cee]$ in a condensed target.

of a free $t\mu$ atom, \mathbf{r}_1 is the $t\mu$ internal vector, and \mathcal{H}_{DC} denotes the internal Hamiltonian of a free D_2 molecule. It is assumed that $dt\mu$ formation takes place in $t\mu$ collision with the l th molecule DC. The position of its mass center in the target frame is denoted by \mathbf{R}_l ; $\boldsymbol{\varrho}_1$ is a vector connecting the nuclei inside this molecule. Function V stands for the potential of the $t\mu$ -DC interaction [13] that leads to resonant $dt\mu$ formation. Vector $\boldsymbol{\varrho}_2$ connects the $t\mu$ and the DC centers of masses. We neglect contributions to potential V from the molecules other than the l th molecule because we assume here that distances between different molecules in the target are much greater than the DC-molecule size. This assumption is valid for condensed hydrogens under low pressure [27, 28]. The kinetic energy ε of the impinging muonic atom and its momentum \mathbf{k} in the target frame are connected by the relation

$$\varepsilon = k^2 / (2M_{a\mu}).$$

The initial Hamiltonian \mathcal{H} of the condensed hydrogen-isotope target, corresponding to the initial target energy E_0 , has the following form:

$$\mathcal{H} = \sum_j \frac{1}{2M_j} \nabla_{\mathbf{R}_j}^2 + \sum_j \sum_{j' \neq j} U_{jj'}, \quad (9)$$

where \mathbf{R}_j is the position of the j th-molecule CMS (see Fig. 4), $U_{jj'}$ denotes interaction between the j th and j' th molecule, and M_j is the mass of the j th molecule.

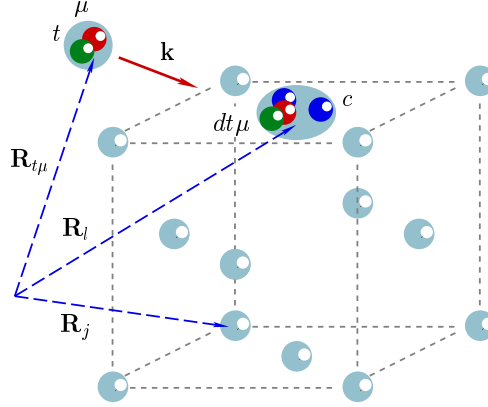


FIG. 4: Position of the impinging $t\mu$ atom with respect to the condensed target.

The coordinate part Ψ_{tot} of the initial wave function of the system can be written as a product

$$\Psi_{\text{tot}} = \psi_{t\mu}^{1S}(\mathbf{r}_1) \psi_{\text{DC}}^{\nu_i K_i}(\boldsymbol{\varrho}_1) \exp(i\mathbf{k} \cdot \mathbf{R}_{t\mu}) |0\rangle, \quad (10)$$

where $|0\rangle$ stands for the initial wave function of the condensed target, corresponding to the total energy E_0 . The eigenfunctions of the operators $H_{t\mu}$ and H_{DC} are denoted by $\psi_{t\mu}^{1S}$ and $\psi_{\text{DC}}^{\nu_i K_i}$, respectively. Using the relation $\mathbf{R}_{t\mu} = \mathbf{R}_l + \boldsymbol{\varrho}_2$, the wave function Ψ_{tot} takes the form

$$\Psi_{\text{tot}} = \psi_{t\mu}^{1S}(\mathbf{r}_1) \psi_{\text{DC}}^{\nu_i K_i}(\boldsymbol{\varrho}_1) \exp(i\mathbf{k} \cdot \boldsymbol{\varrho}_2) \exp(i\mathbf{k} \cdot \mathbf{R}_l) |0\rangle, \quad (11)$$

which is similar to that used in the case of $dt\mu$ formation in a single molecule DC, except the factor $\exp(i\mathbf{k} \cdot \mathbf{R}_l) |0\rangle$. This factor depends only on the CMS positions of the target molecules.

After formation of the $[(dt\mu)cee]$ complex, the total Hamiltonian of the system is well approximated by the operator $\mathcal{H}'_{\text{tot}}$

$$\mathcal{H}_{\text{tot}} \approx \mathcal{H}'_{\text{tot}} = \mathcal{H}_{dt\mu}(\mathbf{r}, \mathbf{R}) + \mathcal{H}_{\text{cplx}}(\boldsymbol{\varrho}) + V(\boldsymbol{\varrho}, \mathbf{r}, \mathbf{R}) + \widetilde{\mathcal{H}}, \quad (12)$$

where $\mathcal{H}_{dt\mu}$ is the internal Hamiltonian of the $dt\mu$ and vectors \mathbf{r} and \mathbf{R} denote its Jacobi coordinates. Relative motion of the $dt\mu$ and nucleus c in the complex is described by a Hamiltonian $\mathcal{H}_{\text{cplx}}$, which depends on the corresponding internal vector $\boldsymbol{\varrho}$. The final Hamiltonian $\widetilde{\mathcal{H}}$ of the target is

$$\begin{aligned} \widetilde{\mathcal{H}} &= \frac{1}{2M_{\text{cplx}}} \nabla_{R_l}^2 + \sum_{j \neq l} \frac{1}{2M_j} \nabla_{R_j}^2 + \sum_j \sum_{j' \neq j} U_{jj'} \\ &= \mathcal{H} + \Delta\mathcal{H}, \end{aligned} \quad (13)$$

where

$$\Delta\mathcal{H} = -\alpha \frac{1}{2M_{\text{DC}}} \nabla_{R_l}^2, \quad \alpha \equiv 1 - \frac{M_{\text{DC}}}{M_{\text{cplx}}} \lesssim \frac{1}{2}, \quad (14)$$

M_{cplx} is the mass of the complex, and $M_{\text{DC}} = M_l$ is the mass of the DC molecule. A small perturbation of potential V , due to replacement of the DC center of mass by that of the complex, is neglected here. The eigenfunction and eigenvalue of $\widetilde{\mathcal{H}}$ are denoted by $|\widetilde{n}\rangle$ and \widetilde{E}_n , respectively. The coordinate part Ψ'_{tot} of the final total wave function of the system is

$$\Psi'_{\text{tot}} = \psi_{dt\mu}^{Jv}(\mathbf{r}, \mathbf{R}) \psi_{\text{cplx}}^{\nu_f K_f}(\boldsymbol{\varrho}) |\widetilde{n}\rangle, \quad (15)$$

where $\psi_{dt\mu}^{Jv}$ and $\psi_{\text{cplx}}^{\nu_f K_f}$ stand for eigenfunctions of the corresponding Hamiltonians $H_{dt\mu}$ and H_{cplx} .

For the initial $|0\rangle$ and final $|\widetilde{n}\rangle$ target states and for a fixed $t\mu$ spin F , the energy-dependent $dt\mu$ -formation rate $\lambda_{\nu_i K_i, \nu_f K_f}^{SF}(\varepsilon)$ is calculated using the equation

$$\begin{aligned} \lambda_{\nu_i K_i, \nu_f K_f}^{SF} &= N_{\text{mol}} B_{if} |\mathcal{A}_{i0,fn}|^2 \\ &\times \frac{\Gamma_S}{(\varepsilon + E_0 - \varepsilon_{if}^0 - \widetilde{E}_n)^2 + \frac{1}{4}\Gamma_S^2}, \end{aligned} \quad (16)$$

with the resonance condition

$$\varepsilon + E_0 = \varepsilon_{if}^0 + \widetilde{E}_n. \quad (17)$$

Equation (16) is analogical to the Breit-Wigner form (6) used for a free molecule. However, the transition-matrix element is now given by

$$\mathcal{A}_{i0,fn} = \langle \Psi'_{\text{tot}} | V | \Psi_{\text{tot}} \rangle. \quad (18)$$

By virtue of Eqs. (11) and (15), the matrix element (18) can be written as a product

$$\mathcal{A}_{i0,fn} = \langle \widetilde{n} | \exp(i\mathbf{k} \cdot \mathbf{R}_l) | 0 \rangle V_{if}(\varepsilon), \quad (19)$$

where $V_{if}(\varepsilon)$ is the energy-dependent transition-matrix element calculated for a single molecule [13]. Averaging the rate (16) over a distribution ρ_{n_0} of the initial target states at a given temperature T and summing over the final target states leads to

$$\begin{aligned} \lambda_{\nu_i K_i, \nu_f K_f}^{SF} &= N_{\text{mol}} B_{if} |V_{if}|^2 \Gamma_S \\ &\times \sum_{n, n_0} \rho_{n_0} \frac{|\langle \widetilde{n} | \exp(i\mathbf{k} \cdot \mathbf{R}_l) | 0 \rangle|^2}{(\varepsilon + E_0 - \varepsilon_{if}^0 - \widetilde{E}_n)^2 + \frac{1}{4}\Gamma_S^2}. \end{aligned}$$

Factor B_{if} is due to averaging over the initial projections and summation over the final spin projections and over the rotational-vibrational quantum numbers. The equation above can be written down in the integral form

$$\begin{aligned} \lambda_{\nu_i K_i, \nu_f K_f}^{SF} &= N_{\text{mol}} B_{if} |V_{if}|^2 \Gamma_S \\ &\times \sum_{n, n_0} \rho_{n_0} |\langle \widetilde{n} | \exp(i\mathbf{k} \cdot \mathbf{R}_l) | 0 \rangle|^2 \\ &\times \int_{-\infty}^{\infty} dE \frac{\delta(E - \widetilde{E}_n + E_0)}{(\varepsilon - \varepsilon_{if}^0 - E)^2 + \frac{1}{4}\Gamma_S^2}. \end{aligned}$$

Now we introduce a time variable t to eliminate the δ function in the equation above and then we involve time-dependent operators, which is familiar in scattering theory [41, 42]. Using the Fourier expansion of the δ function one obtains

$$\lambda_{\nu_i K_i, \nu_f K_f}^{SF} = \frac{1}{2\pi} N_{\text{mol}} B_{if} |V_{if}|^2 \Gamma_S \int_{-\infty}^{\infty} dt \sum_{n, n_0} \rho_{n_0} |\langle \tilde{n} | \exp(i\mathbf{k} \cdot \mathbf{R}_l) | 0 \rangle|^2 \exp[it(\tilde{E}_n - E_0)] \\ \times \int_{-\infty}^{\infty} dE \frac{\exp(-iEt)}{(\varepsilon - \varepsilon_{if}^0 - E)^2 + \frac{1}{4}\Gamma_S^2},$$

which, after integration over E , gives

$$\lambda_{\nu_i K_i, \nu_f K_f}^{SF} = N_{\text{mol}} B_{if} |V_{if}|^2 \int_{-\infty}^{\infty} dt \exp \left[-it(\varepsilon - \varepsilon_{if}^0) - \frac{1}{2}\Gamma_S |t| \right] \sum_{n, n_0} \rho_{n_0} \\ \times \langle 0 | \exp(-i\mathbf{k} \cdot \mathbf{R}_l) | \tilde{n} \rangle \langle \tilde{n} | \exp(it\tilde{E}_n) \exp(i\mathbf{k} \cdot \mathbf{R}_l) \exp(-itE_0) | 0 \rangle. \quad (20)$$

The matrix element in Eq. (20) can be expressed as follows

$$\langle \tilde{n} | \exp(it\tilde{E}_n) \exp(i\mathbf{k} \cdot \mathbf{R}_l) \exp(-itE_0) | 0 \rangle = \langle \tilde{n} | \exp(it\tilde{\mathcal{H}}) \exp(i\mathbf{k} \cdot \mathbf{R}_l) \exp(-it\mathcal{H}) | 0 \rangle \\ = \langle \tilde{n} | \exp(it\tilde{\mathcal{H}}) \exp(-it\mathcal{H}) \exp(it\mathcal{H}) \exp(i\mathbf{k} \cdot \mathbf{R}_l) \exp(-it\mathcal{H}) | 0 \rangle \\ = \langle \tilde{n} | \exp(it\tilde{\mathcal{H}}) \exp(-it\mathcal{H}) \exp[i\mathbf{k} \cdot \mathbf{R}_l(t)] | 0 \rangle,$$

where $\mathbf{R}_l(t)$ denotes the Heisenberg operator

$$\mathbf{R}_l(t) = \exp(it\mathcal{H}) \mathbf{R}_l \exp(-it\mathcal{H}),$$

defined for all l and t .

Employing the identity $\sum_n |\tilde{n}\rangle \langle \tilde{n}| = 1$ in Eq. (20) we obtain

$$\lambda_{\nu_i K_i, \nu_f K_f}^{SF} = 2\pi N_{\text{mol}} B_{if} |V_{if}|^2 \mathcal{S}_{\text{res}}(\mathbf{k}, \varepsilon - \varepsilon_{if}^0), \quad (21)$$

where \mathcal{S}_{res} is the *resonance response function*

$$\mathcal{S}_{\text{res}}(\mathbf{k}, \varepsilon - \varepsilon_{if}^0) \equiv \frac{1}{2\pi} \int_{-\infty}^{\infty} dt \exp \left[-it(\varepsilon - \varepsilon_{if}^0) - \frac{1}{2}\Gamma_S |t| \right] \\ \times \mathcal{Y}_{\text{res}}(\mathbf{k}, t). \quad (22)$$

$\mathcal{Y}_{\text{res}}(\mathbf{k}, t)$ denotes here the *resonance correlation function* defined below

$$\mathcal{Y}_{\text{res}}(\mathbf{k}, t) \equiv \langle \exp[-i\mathbf{k} \cdot \mathbf{R}_l(0)] \exp(it\tilde{\mathcal{H}}) \\ \times \exp(-it\mathcal{H}) \exp[i\mathbf{k} \cdot \mathbf{R}_l(t)] \rangle_T, \quad (23)$$

where $\langle \dots \rangle_T$ stands for the quantum-mechanical and statistical averaging at temperature T .

On substitution $\tilde{\mathcal{H}} = \mathcal{H}$ and $\Gamma_S = 0$ in the equations above, we recover the well-known incoherent response function $\mathcal{S}_{\text{res}} = \mathcal{S}_i$, which describes incoherent neutron scattering in condensed matter [25, 43]. The approximation $\tilde{\mathcal{H}} = \mathcal{H}$ is valid when the mass of an absorbed particle is much smaller than the mass of a target atom or a molecule. This is

a common and good approximation when neutron absorption by a much heavier nucleus is considered. However, the difference $\Delta\mathcal{H}$ between the Hamiltonians $\widetilde{\mathcal{H}}$ and \mathcal{H} cannot be neglected in the case of muonic molecule formation since the mass of muonic hydrogen atom is comparable with that of hydrogen isotope molecule.

The partial width $\Gamma_{\nu_f K_f, \nu_i K_i}^{SF'}$ of back decay of the complex, bound in a condensed target, is given by the expression analogical to Eq. (1)

$$\Gamma_{\nu_f K_f, \nu_i K_i}^{SF'} = 2\pi A_{if} \int \frac{d^3 k}{(2\pi)^3} |\mathcal{A}_{i0,fn}|^2 \delta(\varepsilon_{if}^0 + \widetilde{E}_n - \varepsilon - E_0). \quad (24)$$

Using the Fourier expansion of the δ function and proceeding as in the case of quasis resonant formation process we obtain

$$\Gamma_{\nu_f K_f, \nu_i K_i}^{SF'} = 2\pi A_{if} \int \frac{d^3 k}{(2\pi)^3} |V_{if}(\varepsilon)|^2 \widetilde{\mathcal{S}}_{\text{res}}(\mathbf{k}, \varepsilon_{if}^0 - \varepsilon), \quad (25)$$

where $\widetilde{\mathcal{S}}_{\text{res}}$ denotes function (22) calculated for the initial state $|\widetilde{n}\rangle$, with Γ_S set to zero.

In order to compare the calculated formation rates with experiments, the summed formation rates $\lambda_{K_i}^F(\varepsilon)$ are introduced

$$\lambda_{K_i}^F = \sum_{\nu_f, K_f, S} \lambda_{\nu_i K_i \nu_f K_f}^{SF}, \quad \nu_i = 0. \quad (26)$$

In simulations of muon-catalyzed fusion involving energy-dependent rates of various processes the “absolute” formation rates (26) should be used. However, it is convenient to consider an effective formation rate $\bar{\lambda}_{K_i}^F(\varepsilon)$ that leads to dt fusion in the muonic-molecular complex. The fusion probability depends on decay of the created complex into the two initial objects: the muonic atom and the hydrogen-isotope molecule. This process competes with transitions leading to dt fusion inside the complex. If the lifetime of the complex ($\lesssim 1$ ns) is much shorter than its rotational relaxation time, decay takes place back to the initial channel. When these times are comparable, it is necessary to include back decay from lower rotational states of the complex. In particular, in the limit of very fast rotational relaxation, back decay from the ground rotational state $K_f = 0$ is dominant. Such situation takes place in dense targets, where interactions of the complex with neighboring molecules lead to fast rotational deexcitation. Calculations presented in Refs. [32, 33] show that rotational relaxation of the complex, via scattering on neighboring hydrogenic molecules, is fast at the liquid hydrogen density. The effective formation rate is then

$$\bar{\lambda}_{K_i}^F = \sum_{K_f, S} \lambda_{\nu_i K_i \nu_f K_f}^{SF} \mathcal{P}_{\text{fus}}^S, \quad \nu_i = 0, \quad (27)$$

where $\mathcal{P}_{\text{fus}}^S$ is the fusion fraction

$$\mathcal{P}_{\text{fus}}^S = \lambda_f / \Gamma_S$$

and the back-decay rate λ_{bck}^S is given by

$$\lambda_{\text{bck}}^S = \sum_{F'} \Gamma_{SF'}, \quad \Gamma_{SF'} = \sum_{\nu_i'} \sum_{K_i', K_f=0} \Gamma_{\nu_f K_f, \nu_i' K_i'}^{SF'}.$$

It is assumed here that the vibrational level ν_f of the complex is not changed during its lifetime. Though calculations of vibrational relaxation of the muonic molecular systems in condensed targets have not been performed yet, the available data [28] concerning $\nu = 1 \rightarrow 0$ relaxation time for H_2 in solid ($8 \mu\text{s}$) and liquid ($12 \mu\text{s}$ at 14.2 K) hydrogen suggest that such times are much greater than the lifetime of the muonic molecular complex.

B. Formation in a solid in the strong-binding limit

Evaluation of the response function \mathcal{S}_{res} is difficult, in a general case. The first problem is that the operators $\mathbf{R}_l(t)$, \mathcal{H} , and $\Delta\mathcal{H}$ in Eq. (23) do not commute. However, when muonic molecule formation takes place at energies significantly smaller than the mean kinetic energy \mathcal{E}_T of molecule DC, the perturbation operator (14) is well approximated by its mean value

$$\begin{aligned}\Delta\mathcal{H} &\approx \langle 0|\Delta\mathcal{H}|0\rangle = -\alpha \langle \nabla_{R_l}^2/(2M_{\text{DC}})\rangle_T \\ &= -\alpha \mathcal{E}_T \equiv \Delta\varepsilon_{if} < 0.\end{aligned}\tag{28}$$

Using this approximation in Eq. (23) we obtain

$$\begin{aligned}\mathcal{Y}_{\text{res}}(\mathbf{k}, t) &\approx \exp(it\Delta\varepsilon_{if}) \langle \exp[-i\mathbf{k} \cdot \mathbf{R}_l(0)] \exp[i\mathbf{k} \cdot \mathbf{R}_l(t)] \rangle_T \\ &= \exp(it\Delta\varepsilon_{if}) \mathcal{Y}_l(\mathbf{k}, t).\end{aligned}$$

Thus, function \mathcal{Y}_{res} reduces to the standard incoherent correlation function $\mathcal{Y}_l(\mathbf{k}, t)$ [43], multiplied by the factor $\exp(it\Delta\varepsilon_{if})$ describing a variation of the mean target energy due to its mass change. Hence, the formation rate (21) can be written down as follows:

$$\begin{aligned}\lambda_{\nu_i K_i, \nu_f K_f}^{SF} &= N_{\text{mol}} B_{if} |V_{if}|^2 \int_{-\infty}^{\infty} dt \mathcal{Y}_l(\mathbf{k}, t) \\ &\times \exp\left[-it(\varepsilon - \varepsilon_{if}) - \frac{1}{2}\Gamma_S|t|\right],\end{aligned}\tag{29}$$

ε_{if} being the resonance energy in the condensed target

$$\varepsilon_{if} = \varepsilon_{if}^0 + \Delta\varepsilon_{if}.\tag{30}$$

This energy is shifted by $\Delta\varepsilon_{if} < 0$, compared to the free-molecule resonance energy ε_{if}^0 . Note that such a resonant-energy shift was neglected in Refs. [23, 24], where absorption of neutrons and γ -rays by heavy nuclei were considered. An estimation of the shift in the case of γ emission from a nucleus bound in a solid, similar to Eq. (28) was given in Ref. [44].

Using the following relation between $\mathcal{Y}_l(\boldsymbol{\kappa}, t)$ and the standard single-particle function $G_s(\mathbf{r}, t)$ [43]:

$$G_s(\mathbf{r}, t) = \frac{1}{(2\pi)^3} \int d^3\kappa \exp(-i\boldsymbol{\kappa} \cdot \mathbf{r}) \frac{1}{N_{\text{mol}}} \sum_l \mathcal{Y}_l(\boldsymbol{\kappa}, t),$$

the rate (29) can be expressed as a time and space Fourier transform

$$\begin{aligned}\lambda_{\nu_i K_i, \nu_f K_f}^{SF} &= N_{\text{mol}} B_{if} |V_{if}|^2 \int d^3r dt G_s(\mathbf{r}, t) \\ &\times \exp\left[i(\boldsymbol{\kappa} \cdot \mathbf{r} - \omega t) - \frac{1}{2}\Gamma_S|t|\right],\end{aligned}\tag{31}$$

where the momentum transfer $\boldsymbol{\kappa}$ and the energy transfer ω to the target are

$$\boldsymbol{\kappa} = \mathbf{k}, \quad \omega = \varepsilon - \varepsilon_{if}. \quad (32)$$

Analogously, the back-decay width (25) in the strong-binding limit can be expressed by $G_s(\mathbf{r}, t)$ or by the incoherent response function \mathcal{S}_i introduced by Van Hove

$$\mathcal{S}_i(\boldsymbol{\kappa}, \omega) = \frac{1}{2\pi} \int d^3r dt G_s(\mathbf{r}, t) \exp[i(\boldsymbol{\kappa} \cdot \mathbf{r} - \omega t)].$$

As a result, Eq. (25) takes a simpler form

$$\Gamma_{\nu_f K_f, \nu_i K_i}^{SF'} = 2\pi A_{if} \int \frac{d^3k}{(2\pi)^3} |V_{if}(\varepsilon)|^2 \tilde{\mathcal{S}}_i(\mathbf{k}, \omega'), \quad (33)$$

in which

$$\omega' = \tilde{\varepsilon}_{if} - \varepsilon, \quad \tilde{\varepsilon}_{if} = \varepsilon_{if}^0 + \Delta\tilde{\varepsilon}_{if}. \quad (34)$$

and

$$\Delta\tilde{\varepsilon}_{if} \equiv \langle \tilde{n} | \Delta\mathcal{H} | \tilde{n} \rangle = - (M_{\text{cplx}}/M_{\text{DC}} - 1) \tilde{\mathcal{E}}_T < 0, \quad (35)$$

$\tilde{\mathcal{E}}_T$ being the mean kinetic energy of the complex in the condensed target.

The equations derived above show that calculation of the formation and back-decay rates in the low-energy limit reduces to evaluation of the standard incoherent correlation functions, which are well-known in the neutron scattering theory. In particular, for a perfect gas or a harmonic solid composed of particles with mass M_{mol} , these functions take the simple Gaussian shapes [25, 43]

$$G_s(\mathbf{r}, t) = \left[\frac{M_{\text{mol}}}{2\pi\gamma(t)} \right]^{3/2} \exp \left[-\frac{M_{\text{mol}}}{2\gamma(t)} r^2 \right], \quad (36)$$

$$\mathcal{Y}_l(\boldsymbol{\kappa}, t) = \exp \left[-\gamma(t) \frac{\kappa^2}{2M_{\text{mol}}} \right]. \quad (37)$$

For a solid with a cubic Bravais structure, function $\gamma(t)$ is

$$\gamma(t) = \int_0^\infty dw \frac{Z(w)}{w} \left\{ \coth(\tfrac{1}{2}\beta_T w) [1 - \cos(wt)] - i \sin(wt) \right\}, \quad (38)$$

where the normalized density of vibrational states $Z(w)$ has the following properties:

$$\int_0^\infty dw Z(w) = 1, \quad Z(w) = 0 \quad \text{for } w > w_{\text{max}}, \quad (39)$$

$$Z(-w) \equiv Z(w)$$

and $\beta_T = (k_B T)^{-1}$ (k_B is Boltzmann's constant).

Solid hydrogens under low pressure, used for studies of muonic atoms and molecules, are quantum molecular crystals. They have the Bravais fcc polycrystalline structure or the hcp polycrystalline structure [27, 28], for which Eqs. (36) and (37) are fair approximations. As

a result, on substitution $M_{\text{mol}} = M_{\text{DC}}$, we obtain the phonon expansion for the resonant-formation rate

$$\lambda_{\nu_i K_i, \nu_f K_f}^{SF} = N_{\text{mol}} B_{if} |V_{if}|^2 \exp(-2W) \times \left[\frac{\Gamma_S}{\omega^2 + \frac{1}{4}\Gamma_S^2} + 2\pi \sum_{n=1}^{\infty} g_{\Gamma n}(\omega) \frac{(2W)^n}{n!} \right], \quad (40)$$

in which

$$g_{\Gamma 1}(w) = \frac{1}{2\pi} \int_{-\infty}^{\infty} dz \frac{\Gamma_S}{z^2 + \frac{1}{4}\Gamma_S^2} g_1(z + w, T), \quad (41)$$

$$g_{\Gamma n}(w) = \int_{-\infty}^{\infty} dw' g_{\Gamma 1}(w - w') g_{n-1}(w'),$$

and

$$g_1(w) = \frac{1}{\gamma(\infty)} \frac{Z(w)}{w} [n_B(w) + 1],$$

$$g_n(w) = \int_{-\infty}^{\infty} dw' g_1(w - w') g_{n-1}(w'), \quad (42)$$

$$\int_{-\infty}^{\infty} dw g_n(w) = 1.$$

The exponent $2W$ of the Debye-Waller factor $\exp(-2W)$, familiar in the theory of neutron scattering, is

$$2W(\kappa^2) = \frac{\kappa^2}{2M_{\text{mol}}} \gamma(\infty)$$

$$= \frac{\kappa^2}{2M_{\text{mol}}} \int_0^{\infty} dw \frac{Z(w)}{w} \coth\left(\frac{1}{2}\beta_T w\right),$$

where $\gamma(\infty)$ stands for the limit of $\gamma(t)$ at $t \rightarrow \infty$. Function $n_B(w)$ denotes the Bose factor

$$n_B(w) = [\exp(\beta_T w) - 1]^{-1}. \quad (43)$$

The Breit-Wigner term in expansion (40) describes recoil-less resonant formation. The sum with higher powers of $2W$ correspond to quasis resonant muonic molecule formation with simultaneous phonon creation or annihilation. In particular, the term with $n = 1$ describes formation connected with creation or annihilation of one phonon. In the strong-binding limit $2W \ll 1$, only few lowest terms in expansion (40) are significant. The phonon expansion (40) is more general than an analogous expansion in Ref. [24], which includes the Breit-Wigner factor only in the nonphonon term. This factor should be taken into account also in the phonon terms, unless the natural resonance width is much smaller than w_{max} . For $2W \gtrsim 1$, the approximation (28) and Eq. (40) are no longer valid.

When $dd\mu$ formation is concerned, the resonances are very narrow. Thus, in this case, the limit $\Gamma_S \rightarrow 0$ is practically reached. The Breit-Wigner factor tends to the δ -function profile and $g_{\Gamma n} \rightarrow g_n$. As a result, Eq. (40) takes for $dd\mu$ a simpler form, derived in Ref. [29]

$$\lambda_{\nu_i K_i, \nu_f K_f}^{SF} = 2\pi N B_{if} |V_{if}|^2 \exp(-2W) \times \left[\delta(\omega) + \sum_{n=1}^{\infty} g_n(\omega) \frac{(2W)^n}{n!} \right]. \quad (44)$$

A phonon expansion can also be applied for estimation of the back-decay rate. After integration of Eq. (33) over direction of \mathbf{k} one obtains

$$\Gamma_{\nu_f K_f, \nu_i K_i}^{SF'} = \frac{A_{if}}{\pi} \int_0^\infty dk k^2 |V_{if}(\varepsilon)|^2 \tilde{\mathcal{S}}_i(k^2, \omega').$$

Substitution of the phonon expansion for $\tilde{\mathcal{S}}_i$ into equation above and then integration of the δ -function term lead to

$$\begin{aligned} \Gamma_{\nu_f K_f, \nu_i K_i}^{SF'} = \frac{A_{if}}{\pi} & \left[M_{a\mu} \tilde{k}_{if} |V_{if}(\tilde{\varepsilon}_{if})|^2 \exp(-2\tilde{W}_{if}) \right. \\ & + \sum_{n=1}^{\infty} \int_0^\infty dk k^2 |V_{if}(\varepsilon)|^2 \exp(-2\tilde{W}) \\ & \left. \times g_n(\omega') \frac{(2\tilde{W})^n}{n!} \right], \end{aligned} \quad (45)$$

in which

$$\begin{aligned} 2\tilde{W} &= \frac{k^2}{2M_{\text{cplx}}} \tilde{\gamma}(\infty), \quad 2\tilde{W}_{if} = 2\tilde{W}(\tilde{k}_{if}), \\ \text{and } \tilde{k}_{if} &= \sqrt{2M\tilde{\varepsilon}_{if}} \end{aligned} \quad (46)$$

are calculated for the harmonic lattice with the bound muonic molecular complex. Note that Eq. (45) is valid only if a main contribution to the integral comes from small k .

C. Formation in the weak-binding limit

When the incident momentum of the muonic atom is large, the formation time of a muonic molecule is short compared to the characteristic time scale of the dynamic response of the bulk target. Thus, a contribution to the response function (22) from short times is dominant. As a result, it is sufficient to keep only linear terms in t while evaluating an asymptotic form of the correlation function $\mathcal{Y}_{\text{res}}(\mathbf{k}, t)$. In calculations, we shall use the following operator relation:

$$\exp(\hat{A}) \exp(\hat{B}) = \exp(\hat{A} + \hat{B} + \hat{C}), \quad (47)$$

where

$$\begin{aligned} \hat{C} &= \frac{1}{2}[\hat{A}, \hat{B}] + \frac{1}{12}[[\hat{A}, \hat{B}], \hat{B}] + \frac{1}{12}[[\hat{B}, \hat{A}], \hat{A}] \\ &+ \frac{1}{24}[[[\hat{B}, \hat{A}], \hat{A}], \hat{B}] + \dots \end{aligned}$$

Operator $\hat{C} = 0$ only if \hat{A} and \hat{B} are commuting operators.

The operators $\Delta\mathcal{H}$ and \mathcal{H} , defined by Eqs. (9) and (13), do not commute and the operator \hat{C} in the expression

$$\exp\{it(\mathcal{H} + \Delta\mathcal{H})\} \exp(-it\mathcal{H}) = \exp(it\Delta\mathcal{H} + \hat{C})$$

turns out to be a sum containing higher powers of t . Since in this approximation we restrict to terms linear with respect to t and to the parameter $\alpha \lesssim \frac{1}{2}$, the operator \hat{C} in the relation above can be neglected and thus the correlation function takes the form

$$\mathcal{Y}_{\text{res}}(\mathbf{k}, t) = \left\langle \exp\{-i\mathbf{k} \cdot \mathbf{R}_l(0)\} \exp(it\Delta\mathcal{H}) \times \exp\{i\mathbf{k} \cdot \mathbf{R}_l(t)\} \right\rangle_T. \quad (48)$$

Now we involve the basic approximation

$$\mathbf{R}_l(t) \approx \mathbf{R}(0) + (\mathbf{P}_l/M_{\text{DC}})t, \quad (49)$$

where \mathbf{P}_l denotes the momentum operator of the l th molecule. This approximation is valid for $t \rightarrow 0$. After substitution of Eq. (49) in Eq. (48) and multiple use of the Eq. (47) we have

$$\begin{aligned} \mathcal{Y}_{\text{res}}(\mathbf{k}, t) \approx & \exp\left(it\frac{k^2}{2M_{\text{cplx}}}\right) \left\langle \exp\left(-it\alpha\frac{P_l^2}{2M_{\text{DC}}}\right) \right\rangle_T \\ & \times \left\langle \exp\left(it\frac{\mathbf{k} \cdot \mathbf{P}_l}{M_{\text{cplx}}}\right) \right\rangle_T, \end{aligned}$$

Since the argument of the second exponential is small, we can use the following approximation:

$$\begin{aligned} \left\langle \exp\left(-it\alpha\frac{P_l^2}{2M_{\text{DC}}}\right) \right\rangle_T & \approx \exp\left(-it\alpha\left\langle\frac{P_l^2}{2M_{\text{DC}}}\right\rangle_T\right) \\ & = \exp(it\Delta\varepsilon_{if}) \end{aligned}$$

which involves the resonance-energy shift (28). Substitution of the above equations in Eq. (22), with the definitions (30) and (32) taken into account, leads to

$$\begin{aligned} \mathcal{S}_{\text{res}}(\boldsymbol{\kappa}, \omega) = & \frac{1}{2\pi} \int_{-\infty}^{\infty} dt \exp\left[-i\omega t - \frac{1}{2}\Gamma_S|t| + it\frac{\kappa^2}{2M_{\text{cplx}}}\right] \\ & \times \left\langle \exp\left(it\frac{\boldsymbol{\kappa} \cdot \mathbf{P}_l}{M_{\text{cplx}}}\right) \right\rangle_T \end{aligned} \quad (50)$$

When the motion of the molecule DC is well described by an isotropic harmonic potential, the Bloch identity

$$\langle \exp \hat{Q} \rangle_T = \exp\left(\frac{1}{2}\langle \hat{Q}^2 \rangle_T\right) \quad (51)$$

may be applied for an operator \hat{Q} being a linear combination of the Bose operators of creation and annihilation. Since momentum \mathbf{P}_l can be expressed by such operators (see e.g., Ref [43]), we have

$$\begin{aligned} \left\langle \exp\left(it\frac{\boldsymbol{\kappa} \cdot \mathbf{P}_l}{M_{\text{cplx}}}\right) \right\rangle_T & = \exp\left(-\frac{1}{4}\Delta_{\text{res}}^2\right), \\ \Delta_{\text{res}}^2 & = \frac{2}{M_{\text{cplx}}^2} \langle (\boldsymbol{\kappa} \cdot \mathbf{P}_l)^2 \rangle_T. \end{aligned} \quad (52)$$

In the case of cubic symmetry,

$$\langle (\boldsymbol{\kappa} \cdot \mathbf{P}_l)^2 \rangle_T = \frac{1}{3} \kappa^2 \langle P_l^2 \rangle_T,$$

and this is a fair approximation even for other lattices. Thus

$$\Delta_{\text{res}}^2 = \frac{2}{3M_{\text{cplx}}^2} \kappa^2 \langle P_l^2 \rangle_T = \frac{8}{3} \frac{M_{\text{DC}}}{M_{\text{cplx}}} \left\langle \frac{P_l^2}{2M_{\text{DC}}} \right\rangle_T \frac{\kappa^2}{2M_{\text{cplx}}},$$

which finally gives the following Doppler width:

$$\Delta_{\text{res}} = 2 \sqrt{\frac{2}{3} \frac{M_{\text{DC}}}{M_{\text{cplx}}} \mathcal{E}_T \omega_R}, \quad (53)$$

with the recoil energy

$$\omega_R = \kappa^2 / (2M_{\text{cplx}}). \quad (54)$$

In the case of a solid hydrogen target, the mean kinetic energy of the bound molecule equals

$$\mathcal{E}_T = \frac{3}{2} \int_0^\infty dw Z(w) w \left[n_{\text{B}}(w) + \frac{1}{2} \right]. \quad (55)$$

This energy is much higher than $\mathcal{E}_T = \frac{3}{2} k_{\text{B}} T$ for a corresponding Maxwellian gas, unless the temperature is sufficiently high. This phenomenon was first taken into account by Lamb [23], in resonant neutron absorption in solid crystals. In particular, for a low-pressure solid or liquid deuterium, $\mathcal{E}_T \approx 5$ meV [45] due to a large zero-point motion of D_2 molecules in a given target. The effective target temperature T_{eff} corresponding to \mathcal{E}_T is then defined as

$$T_{\text{eff}} \equiv \frac{2}{3} k_{\text{B}}^{-1} \mathcal{E}_T. \quad (56)$$

For the considered solid D_2 case, $T_{\text{eff}} \approx 40$ K.

Substitution of Eqs. (52) and (54) in Eq. (50) leads to

$$\begin{aligned} \mathcal{S}_{\text{res}}(\boldsymbol{\kappa}, \omega) = \frac{1}{2\pi} \int_{-\infty}^{\infty} dt \exp \left[-i(\omega - \omega_R)t \right. \\ \left. - \frac{1}{2} \Gamma_S |t| - \frac{1}{4} \Delta_{\text{res}}^2 t^2 \right]. \end{aligned} \quad (57)$$

Then, applying the convolution theorem to the Fourier transform of a product, we obtain the asymptotic form of the resonance response function

$$\begin{aligned} \mathcal{S}_{\text{res}}(\boldsymbol{\kappa}, \omega) = \frac{1}{2\pi^{3/2}} \frac{\Gamma_S}{\Delta_{\text{res}}} \int_{-\infty}^{\infty} \frac{dz}{z^2 + \frac{1}{4} \Gamma_S^2} \\ \times \exp \left[- \left(\frac{z + \omega - \omega_R}{\Delta_{\text{res}}} \right)^2 \right]. \end{aligned} \quad (58)$$

By virtue of Eq. (58), the formation rate (21) in the weak-binding limit takes the form

$$\begin{aligned} \lambda_{\nu_i K_i, \nu_f K_f}^{SF} = N_{\text{mol}} B_{if} |V_{if}|^2 \frac{\Gamma_S}{\Delta_{\text{res}} \sqrt{\pi}} \\ \times \int_{-\infty}^{\infty} \frac{dz}{z^2 + \frac{1}{4} \Gamma_S^2} \exp \left[- \left(\frac{z + \omega - \omega_R}{\Delta_{\text{res}}} \right)^2 \right]. \end{aligned} \quad (59)$$

This equation is similar (apart from the muonic-molecule factor $N_{\text{mol}} B_{if} |V_{if}|^2$) to the expression for resonant absorption of neutrons in a gas target, obtained by Bethe and Placzek [46]. However, the resonance width (53) and recoil energy (54) take into account a change of the target particle mass in the absorption process, which is neglected in their work.

In the limit $\Gamma_S \rightarrow 0$, Eqs. (58) and (59) tend to the following expressions:

$$\mathcal{S}_{\text{res}}(\boldsymbol{\kappa}, \omega) = \frac{1}{\Delta_{\text{res}} \sqrt{\pi}} \exp \left[- \left(\frac{\omega - \omega_R}{\Delta_{\text{res}}} \right)^2 \right] \quad (60)$$

and

$$\begin{aligned} \lambda_{\nu_i K_i, \nu_f K_f}^{SF} &= 2\sqrt{\pi} N_{\text{mol}} B_{if} |V_{if}|^2 \\ &\times \frac{1}{\Delta_{\text{res}}} \exp \left[- \left(\frac{\omega - \omega_R}{\Delta_{\text{res}}} \right)^2 \right], \end{aligned} \quad (61)$$

respectively. Function (60) has the Gaussian form, identical with that used for description of incoherent scattering at large energies. However, the Doppler width (53) and the recoil energy (54) in \mathcal{S}_{res} are different from the corresponding variables

$$\Delta_R = 2\sqrt{\frac{2}{3} \mathcal{E}_T \omega_R} \quad (62)$$

and

$$\omega_R = \kappa^2 / (2M_{\text{mol}}), \quad (63)$$

which determine the asymptotic form of the standard incoherent response function \mathcal{S}_i [43]. Function \mathcal{S}_{res} tends to \mathcal{S}_i if the approximation $M_{\text{cplx}} \approx M_{\text{DC}}$ is valid. However, in the case of muonic molecule formation, this is only a rough approach because the mass of a muonic hydrogen atom is comparable with the mass of a hydrogen isotope molecule. Note that, in the strong-binding limit, mass M_{cplx} enters only the resonance-energy shift (28). The phonon expansion (40) is expressed in terms of $W \sim \kappa^2 / 2M_{\text{DC}}$, not in terms of $\bar{W} \sim \kappa^2 / 2M_{\text{cplx}}$. The reason is that Eq. (40) is valid for small collision energies, when the target molecule is strongly bound in the lattice. Therefore, the momentum is mostly transferred to the whole crystal.

Function (60) can be used for evaluation of the back-decay rate, if large final momenta give main contribution to the integral (25). After integration over direction of \mathbf{k} in Eq. (25), with the asymptotic function (60) inserted, one obtains

$$\begin{aligned} \Gamma_{\nu_f K_f, \nu_i K_i}^{SF'} &= \frac{A_{if}}{\pi^{3/2} \tilde{\Delta}_{\text{res}}} \int_0^\infty dk k^2 |V_{if}(\varepsilon)|^2 \\ &\times \exp \left[- \left(\frac{\omega' - \omega'_R}{\tilde{\Delta}_{\text{res}}} \right)^2 \right], \end{aligned} \quad (64)$$

where ω' is defined by Eq. (34). The parameters $\tilde{\Delta}_{\text{res}}$ and ω'_R are calculated from Eqs. (53) and (54), using the replacements $M_{\text{DC}} \leftrightarrow M_{\text{cplx}}$ and $\mathcal{E}_T \rightarrow \tilde{\mathcal{E}}_T$.

Let us note that Eqs. (58) and (60) are general since they are derived in the impulse approximation (49) without using specific properties of a given target, apart from the single parameter \mathcal{E}_T . Therefore, they are valid for liquid and dense gaseous hydrogens. They can be also used for description of resonant absorption processes other than muonic molecule formation, when a mass change cannot be neglected. In such a case, Γ_S should be replaced by an appropriate natural resonance width.

D. Formation in a solid at intermediate energies

The formation rate calculated according the asymptotic form (59) becomes very inaccurate when the collision energy is much greater than the maximal frequency w_{\max} of a crystal. In particular, this concerns recoil-less formation, which is dominant at lowest energies. Therefore, at the intermediate energies, it is reasonable to represent the formation rate as a sum of the exact nonphonon term from expansion (40) and the subsequent phonon terms, which we obtain below in the impulse approximation. Using Eqs. (47) and (51), it can be shown that the relation

$$\begin{aligned} \mathcal{Y}_l^{\text{res}}(\mathbf{k}, t) &\approx \mathcal{Y}_l(\mathbf{k}, t) \exp(it\Delta\varepsilon_{if}) \\ &\times \exp\left\{\alpha \left[it - \frac{2}{3}(\alpha + 2) \mathcal{E}_T t^2\right] \frac{k^2}{2M_{\text{DC}}}\right\} \end{aligned} \quad (65)$$

is valid in this approximation. Inserting Eqs. (37) and (65) into Eq. (22) we have

$$\begin{aligned} \mathcal{S}_{\text{res}}(\boldsymbol{\kappa}, \omega) &= \frac{1}{2\pi} \int_{-\infty}^{\infty} dt \exp\left\{-it\omega - \frac{1}{2}\Gamma_S|t| \right. \\ &\quad \left. + [-\gamma(t) + i\alpha t \right. \\ &\quad \left. - \frac{2}{3}\alpha(\alpha + 2) \mathcal{E}_T t^2] \frac{\kappa^2}{2M_{\text{DC}}}\right\}. \end{aligned} \quad (66)$$

Substituting the approximation $\gamma(t) \approx -it + \frac{2}{3}\mathcal{E}_T t^2$ for short times into Eq. (66) and integrating over t yields the asymptotic form (58) of the response function. However, we now expand Eq. (66) in powers of κ^2

$$\begin{aligned} \mathcal{S}_{\text{res}}(\boldsymbol{\kappa}, \omega) &= \frac{1}{2\pi} \exp(-2W) \sum_{n=0}^{\infty} \frac{(2W)^n}{n!} \\ &\times \int_{-\infty}^{\infty} dt \exp(-i\omega t - \frac{1}{2}\Gamma_S|t|) [\mathcal{F}(t)]^n, \\ \mathcal{F}(t) &= 1 + i \frac{1+\alpha}{\gamma(\infty)} t - \frac{2}{3} \frac{(1+\alpha)^2}{\gamma(\infty)} \mathcal{E}_T t^2. \end{aligned} \quad (67)$$

Function g_n is defined by Eq. (42). The integral over t is estimated using the exponential approximation to function \mathcal{F}

$$\mathcal{F}(t) \approx \exp(x), \quad x \approx \frac{it}{\gamma_\alpha} - \frac{1}{2} \Delta_\alpha^2 t^2, \quad (68)$$

where x contains only leading terms in t and

$$\gamma_\alpha \equiv \frac{M_{\text{cplx}}}{M_{\text{DC}}} \gamma(\infty), \quad \Delta_\alpha^2 \equiv \frac{4}{3} \frac{M_{\text{DC}}}{M_{\text{cplx}}} \frac{\mathcal{E}_T}{\gamma_\alpha} - \frac{1}{\gamma_\alpha^2}.$$

Then, integration in Eq. (67), using the convolution theorem, leads to

$$\begin{aligned} \mathcal{S}_{\text{res}}(\boldsymbol{\kappa}, \omega) &= \exp(-2W) \left[\frac{1}{2\pi} \frac{\Gamma_S}{\omega^2 + \frac{1}{4}\Gamma_S^2} \right. \\ &\quad \left. + \sum_{n=1}^{\infty} \mathfrak{g}_n(\omega) \frac{(2W)^n}{n!} \right], \end{aligned} \quad (69)$$

where

$$\mathbf{g}_1(\omega) = \frac{1}{2\pi} \int_{-\infty}^{\infty} dz \frac{\Gamma_S}{z^2 + \frac{1}{4}\Gamma_S^2} \frac{Z(z + \omega_\alpha)}{z + \omega_\alpha} \times [n_B(z + \omega_\alpha) + 1], \quad \omega_\alpha = \frac{\omega}{1 + \alpha},$$

and, for $n \geq 2$,

$$\mathbf{g}_n(\omega) = \frac{1}{(2\pi)^{3/2}} \frac{\Gamma_S}{n^{1/2}\Delta_\alpha} \int_{-\infty}^{\infty} dz \frac{1}{z^2 + \frac{1}{4}\Gamma_S^2} \times \exp\left[\frac{(z + \omega - n/\gamma_\alpha)^2}{2n\Delta_\alpha^2}\right].$$

The first term of Eq. (67) has been replaced in (69) by the exact Breit-Wigner term. Also the one-phonon ($n = 1$) contribution to \mathcal{S}_{res} , is replaced here by a more accurate term depending on \mathbf{g}_1 . Function \mathbf{g}_1 is calculated on substitution of the exact function $\gamma(t)$ for a harmonic solid into Eq. (66). Every multiphonon term in Eq. (69) is represented by the convolution of the Breit-Wigner profile with a Gaussian obtained using Eq. (68). It now follows that

$$\lambda_{\nu_i K_i, \nu_f K_f}^{SF} = N_{\text{mol}} B_{if} |V_{if}|^2 \exp(-2W) \times \left[\frac{\Gamma_S}{\omega^2 + \frac{1}{4}\Gamma_S^2} + 2\pi \sum_{n=1}^{\infty} \mathbf{g}_n(\omega) \frac{(2W)^n}{n!} \right]. \quad (70)$$

The form of this expansion is similar to that of Eq. (40), derived in the strong-binding limit. However, functions \mathbf{g}_n are obtained in the impulse approximation and they are different from the corresponding functions $g_{\Gamma n}$ given by Eq. (41). For the one-phonon term, we have $\mathbf{g}_1(\omega) = g_{\Gamma 1}(\omega_\alpha)$, which is the direct result of using the exact $\gamma(t)$ in derivation of \mathbf{g}_1 . Thus, Eqs. (70) and (40) give the same rate at smallest energy transfers. At large ε , when many multiphonon terms are important, the target response no longer displays a rich structure. The rate (70) tends therefore to the simpler form (59), which is characterized by the recoil energy (54) with the correct mass M_{cplx} .

In the limit $\Gamma_S \rightarrow 0$, the rate (70) takes the form similar to Eq. (44)

$$\lambda_{\nu_i K_i, \nu_f K_f}^{SF} = 2\pi N B_{if} |V_{if}|^2 \exp(-2W) \times \left[\delta(\omega) + \sum_{n=1}^{\infty} \mathbf{g}_n(\omega, T) \frac{(2W)^n}{n!} \right], \quad (71)$$

with the expansion coefficients

$$\mathbf{g}_1(\omega) = \frac{Z(\omega_\alpha)}{\omega_\alpha} [n_B(\omega_\alpha) + 1], \quad \mathbf{g}_n(\omega) = \frac{1}{(2\pi n)^{1/2} \Delta_\alpha} \exp\left[\frac{(\omega - n/\gamma_\alpha)^2}{2n\Delta_\alpha^2}\right], \quad n \geq 2.$$

The back-decay rate can be calculated analogously. The result is given by Eq. (45) with functions g_n replaced by the corresponding functions \mathbf{g}_n from Eq. (71). It is also necessary to make the following substitutions: $M_{\text{DC}} \leftrightarrow M_{\text{cplx}}$ and $\mathcal{E}_T \rightarrow \tilde{\mathcal{E}}_T$.

IV. RESULTS OF CALCULATIONS FOR $dt\mu$ FORMATION IN SOLID HYDROGENS

In this Section, the rates of resonant $dt\mu$ formation in solid HD, D₂, and DT are calculated. It is assumed that these targets are kept at zero or low pressures ($\ll 10$ kbar), which corresponds to the TRIUMF or RIKEN-RAL experimental conditions. Measurements of the formation rates at TRIUMF have been performed using energetic (~ 1 eV) beams of $t\mu$ atoms. Therefore, the rates are evaluated here in a wide energy interval $\varepsilon \lesssim 1$ eV. This involves resonant $dt\mu$ formation with simultaneous excitations of a few lowest vibrational levels of the muonic-molecular complex. The values of the rates are given for a normalized target density of 4.25×10^{22} atoms/cm³ (liquid-hydrogen density).

Since exact forms of the vibrational-state distribution $Z(w)$ for the experimental polycrystalline targets are not known, the Debye model of an isotropic solid has been used in the calculations presented below. The values of the Debye temperature Θ_D are taken from the available literature [27, 28].

The resonance energies and energy-dependent transition-matrix elements for isolated target molecules HD, D₂, and DT, calculated according to the method presented in Ref. [47], are the starting point for evaluation of the formation rates in solid hydrogens. The transition-matrix elements are available for the rotational transitions $K_i = 0, 1 \rightarrow K_f = 0, \dots, 9$.

Resonant $dt\mu$ formation in a bound D₂ molecule is the most complicated case. The lowest resonances, corresponding to the vibrational transition $\nu_i = 0 \rightarrow \nu_f = 2$ and different rotational states K_i and K_f , are located in the vicinity of $\varepsilon = 0$ with the radius of a few tens meV. The resonance energies in this region, for a free D₂ molecule and for a D₂ bound in a 3-K solid deuterium, are shown in Table I. In particular, there are several subthreshold reso-

TABLE I: Resonance energies for $dt\mu$ formation in $t\mu$ scattering from a free D₂ molecule (ε_{if}^0) and from a 3-K solid-D₂ target (ε_{if}), corresponding to the vibrational transition $\nu_i = 0 \rightarrow \nu_f = 2$. These energies are given in the corresponding center-of-mass systems.

ε_{if}^0 (meV)	ε_{if} (meV)	F	K_i	K_f	S
-25.66	-27.95	1	1	4	1
-21.25	-23.54	1	0	4	0
-18.66	-20.95	1	1	4	2
-18.25	-20.54	1	0	4	1
-11.25	-13.54	1	0	4	2
-24.15	-26.44	0	1	0	1
-19.28	-21.57	0	1	1	1
-16.74	-19.02	0	0	0	1
-11.86	-14.15	0	0	1	1
-9.547	-11.84	0	1	2	1
-2.133	-4.423	0	0	2	1
5.007	2.718	0	1	3	1
12.42	10.13	0	0	3	1
24.34	22.05	0	1	4	1
31.75	29.46	0	0	4	1

nances that give significant contributions to the low-energy rates, because of wide resonance profiles. The resonance-energy shift (28) for a deuterium target at 3 K is $\Delta\varepsilon_{if} = -2.29$ meV. Resonances in the upper spin state $F = 1$ have much smaller energies than those for $F = 0$ with the same rotational quantum numbers. In particular, the largest values of ε_{if} for $F = 1$, shown in Table I, are due to the excitations $K_i = 0, 1 \rightarrow K_f = 4$. The only matrix elements that do not tend to zero at $\varepsilon \rightarrow 0$ correspond to the dipole transitions $K_i = 0 \rightarrow K_f = 1$ and $K_i = 1 \rightarrow K_f = 0, 2$. For $F = 1$, all these transitions are associated with $\varepsilon_{if} < -50$ meV and thus they give very small contribution to the resonant $dt\mu$ -formation rate. As a result, the low-energy rate is determined mainly by $t\mu$ scattering in the $F = 0$ state. However, even for $F = 0$, the dipole transitions are connected with negative resonance energies, though much closer to $\varepsilon = 0$ than in the $F = 1$ case. The lowest positive resonances appear in the transitions $K_i = 0 \rightarrow K_f = 3, 4$ and $K_i = 1 \rightarrow K_f = 3, 4$. They are characterized by strongly varying transition-matrix elements [47], which is illustrated in Figs. 5 and 6. Let

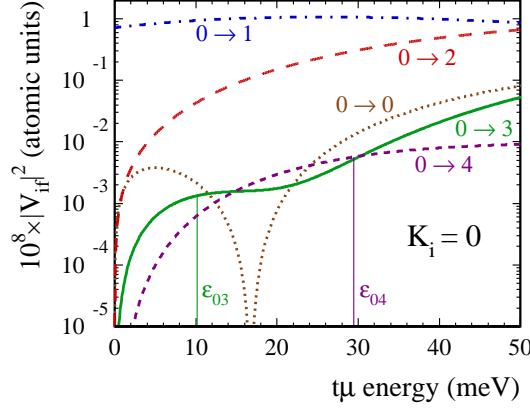


FIG. 5: Matrix elements $|V_{if}(\varepsilon)|^2$ versus $t\mu$ energy for the transitions $K_i = 0 \rightarrow K_f = 0, 1, 2, 3, 4$ and $\nu_i = 0 \rightarrow \nu_f = 2$. The vertical lines denote energies ε_{if} of the lowest resonances. Labels “ $i \rightarrow f$ ” stand for the rotational transitions $K_i \rightarrow K_f$.

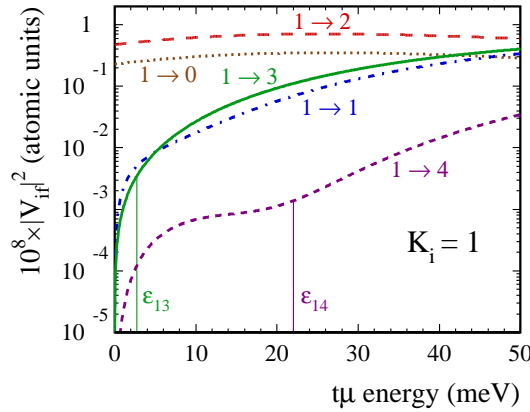


FIG. 6: Matrix elements $|V_{if}(\varepsilon)|^2$ versus $t\mu$ energy for the transitions $K_i = 1 \rightarrow K_f = 0, 1, 2, 3, 4$ and $\nu_i = 0 \rightarrow \nu_f = 2$. Notation is the same as in Fig. 5.

us note that this situation is very different from the $dd\mu$ case, where low-energy formation is determined by the dipole transitions, with the matrix elements slowly varying below a few tens meV [29, 47]. Another difference between the $dd\mu$ and $dt\mu$ case is involved by larger separations of the neighboring $dt\mu$ resonances corresponding to $K_i = 0$ and $K_i = 1$. Therefore, for $dt\mu$ one can expect more pronounced differences between resonant formation in solid ortho- D_2 and para- D_2 than those found for $dd\mu$ case [48]. Most pure-deuterium experiments in μCF have been carried out in targets with the statistical mixture of ortho and parastates (called “normal” deuterium nD_2 , according to the nomenclature used in Ref. [28]).

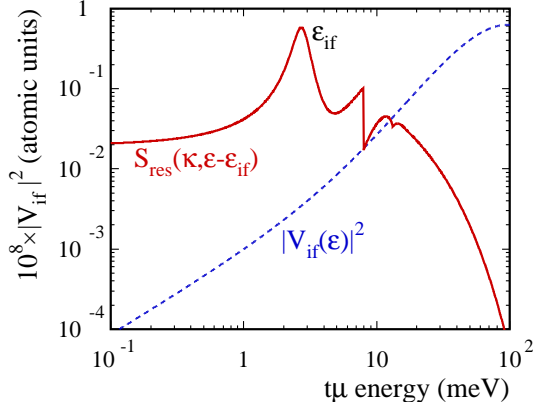


FIG. 7: Transition-matrix element $|V_{if}(\varepsilon)|^2$ for resonant $dt\mu$ formation (transition $\nu_i = 0 \rightarrow \nu_f = 2$, $K_i = 1 \rightarrow K_f = 3$, dashed line) and the response function $\mathcal{S}_{\text{res}}(\kappa, \varepsilon - \varepsilon_{if})$ (in arbitrary units, solid line) for the resonance $F = 0 \rightarrow S = 1$ in 3-K para- D_2 . The peak of the Breit-Wigner term from Eq. (69) is centered at the resonance energy $\varepsilon_{if} = 2.7$ meV.

In Fig. 7 is shown $|V_{if}(\varepsilon)|^2$ for the transition $\nu_i = 0 \rightarrow \nu_f = 2$, $K_i = 1 \rightarrow K_f = 3$, together with the response function (69) for the resonance $F = 0 \rightarrow S = 1$ located at $\varepsilon_{if} = 2.7$ meV. The phonon terms in \mathcal{S}_{res} are calculated assuming $\Gamma_S = 0$, since in this example we want to neglect their convolution with the Breit-Wigner profile. There is a strong contrast between resonant formation of the molecules $dt\mu$ and $dd\mu$ [29] in a solid deuterium. In the $dt\mu$ case, the wide Breit-Wigner peak is not so much pronounced as the narrow recoil-less $dd\mu$ resonances. The matrix element $|V_{if}(\varepsilon)|^2$ raises by a few orders of magnitude within the width of 100 meV of the multiphonon distribution. Thus, the phonon contribution to the $dt\mu$ -formation rate is comparable with the nonphonon one, already above a few meV. This means that a detailed form of the density $Z(w)$ of vibrational lattice states is necessary for accurate calculation of the low-energy $dt\mu$ -formation rate in a solid D_2 . A shape of the phonon spectrum in the energy-dependent rate is strongly distorted, which one sees in Fig. 8 evaluated using Eq. (70). Nevertheless, the one-phonon and two-phonon terms are clearly distinguished in the curve corresponding to para- D_2 . In ortho- D_2 , the resonance with the lowest $\varepsilon_{if} > 0$ is located at 10 meV. Therefore, the Breit-Wigner peak is strongly suppressed by the Debye-Waller factor and the rate is quite flat. At $\varepsilon \rightarrow 0$, the rates are determined by the wings of the Breit-Wigner peaks, because phonon contribution to the rates vanishes when κ approaches zero. For $F = 1$, the main resonances are far from the considered low-energy interval (see Table I). The rates shown in Fig. 9 are thus determined by the Breit-Wigner wings of the deep subthreshold resonances with small contributions from the

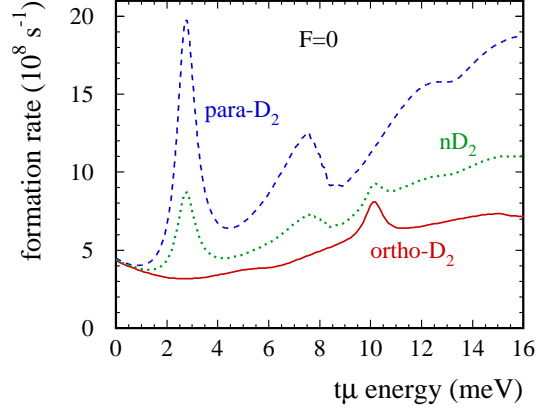


FIG. 8: Low-energy $dt\mu$ -formation rate for $F = 0$ in a 3-K solid nD_2 (“normal” deuterium [28]), $ortho\text{-}D_2$, and $para\text{-}D_2$, calculated using Eq. (70).

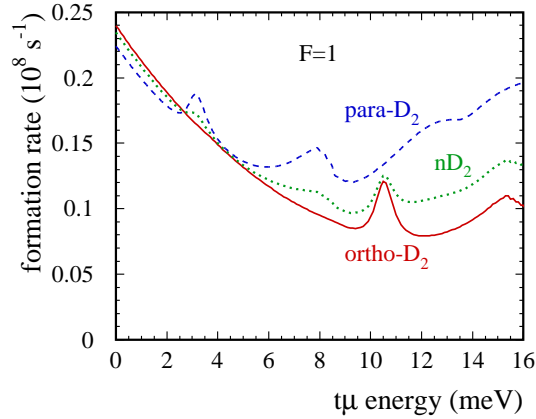


FIG. 9: Low-energy $dt\mu$ -formation rate for $F = 1$ in the same targets as in Fig. 8.

weak resonance ($K_f = 5$) located at $\varepsilon_{if} > 0$. As a result, the formation rates for $F = 1$ are lower by two orders of magnitude than those for $F = 0$.

Resonances in $t\mu$ scattering from D_2 , corresponding to the vibrational excitations $\nu_f \geq 3$ of the $[(dt\mu)dee]$ complex, are located at higher energies $\varepsilon \gtrsim 0.2$ eV. Therefore, they are well described by the asymptotic form (59), which is independent of $Z(w)$. Therefore, the formation rate is determined accurately using only the mean kinetic energy \mathcal{E}_T of a D_2 molecule. The formation rate in a 3-K solid nD_2 is plotted in Fig. 10, for several ν_f . For comparison, in Fig. 11 is shown the $dt\mu$ -formation rate for 3-K gaseous nD_2 . The energy-dependent rate for a perfect deuterium gas has been calculated assuming a 3-K Maxwellian distribution of the D_2 kinetic energy. This rate includes only formation due to two-body $t\mu + D_2$ collisions. The resonant-formation rates presented in Figs. 10 and 11 display a striking difference between the gas and the solid case. At $\varepsilon \rightarrow 0$, the theory developed for two-body collisions in a perfect gas gives a negligible resonant formation rate. This result disagrees with the average formation rates determined by measurements performed in liquid and cold dense-gas targets [3] and in solid [18] targets. The rate for the solid shows a strong contribution from the subthreshold resonances, which leads to a large rate in the limit $\varepsilon \rightarrow 0$. Solid-state

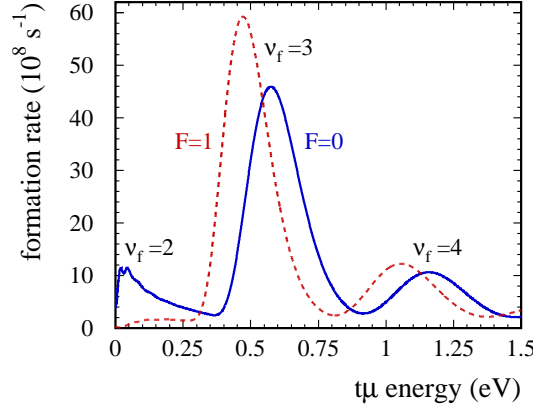


FIG. 10: Resonant $dt\mu$ -formation rate in a 3-K solid nD_2 for $F = 0$ and $F = 1$. The label ν_f denotes the vibrational state of the created $[(dt\mu)dee]$ complex.

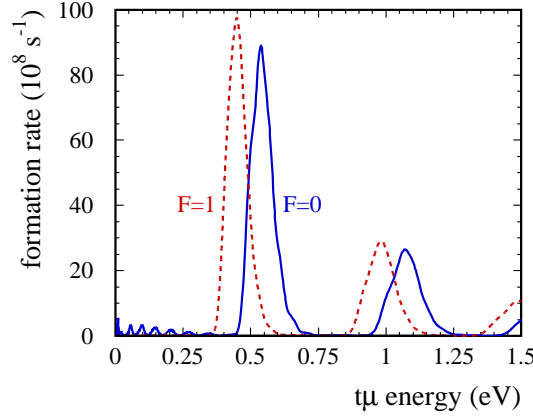


FIG. 11: Resonant $dt\mu$ -formation rate in 3-K gaseous nD_2 calculated in the laboratory frame.

effects are also significant at higher energies. The resonance peaks in the solid are much broader than those in the gas because of a large effective target temperature connected with strong zero-point motion of D_2 in solid deuterium [45]. The widths of the peaks increase with rising recoil energy. However, the centers of higher-energy peaks in the both targets have similar locations since, in the impulse-approximation limit, the recoil energy (54) for the muonic-molecular complex bound in a solid equals to that for the isolated complex. A small difference $\Delta\varepsilon_{if}$ of the resonance energy between the solid and the gas is negligible for $\varepsilon_{if} \gg 1$ meV.

Calculation of the $dt\mu$ -formation rate for a solid HD or DT is simpler than for D_2 since in the HD or DT case there are no significant resonances in the close vicinity of $\varepsilon = 0$. This is caused by different values of the rotational and vibrational quanta for these three molecules. The HD molecule is the lightest one and the resonances connected with $\nu_f = 2$ are situated in HD above 0.1 eV [14, 47]. As a result, contributions from various multiphonon processes to the formation rate plotted in Fig. 12 cannot be distinguished. The resonance peak for $\nu_f = 2$ in HD is the strongest $dt\mu$ resonance found for the three considered molecules. In Fig. 13, the $dt\mu$ -formation rate is shown for a 3-K solid DT target. The lowest peaks,

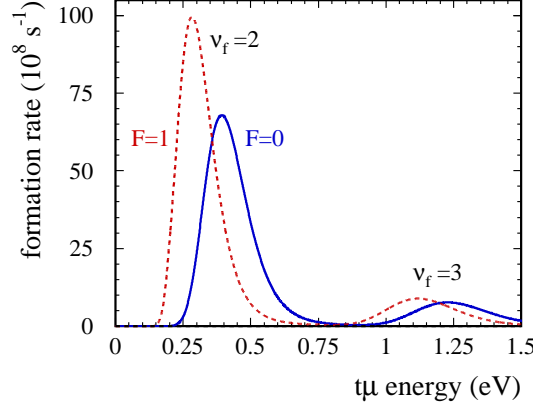


FIG. 12: Resonant $dt\mu$ -formation rate in 3-K solid HD.

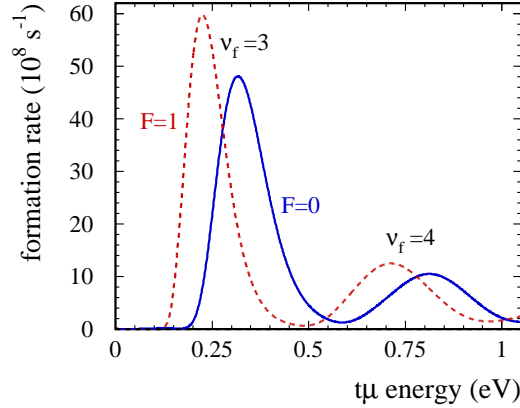


FIG. 13: Resonant $dt\mu$ -formation rate in 3-K solid HT.

which already take the asymptotic form (59), correspond here to $\nu_f = 3$. The rotational and vibrational quanta are smallest for DT, so that the main (lowest K_f) resonances connected with $\nu_f = 2$ are located deeply below $\varepsilon = 0$. Thus, a contribution to the formation rate from the subthreshold resonances is very small and is not apparent in this figure. At 3 K, the effective target temperature T_{eff} , determined by Eqs. (56) and (55), equals about 41 K for HD and 50 K for DT. The resonance shift $\Delta\varepsilon_{if}$ obtained from Eq. (28), equals -2.71 meV in the case of HD and -1.97 meV for DT.

The $dt\mu$ resonances in solid HD and D₂ were directly observed at TRIUMF [19–22] using the energetic $t\mu$ -atom beam and time-of-flight techniques. However, Monte Carlo simulations (see e.g., Ref. [49]) were employed for interpretation of the experimental data. Such a procedure was indispensable since the time-of-flight spectra cannot be uniquely inverted because of the geometry used and the energy loss of $t\mu$ atoms in the reaction layer, prior to resonant formation of the muonic-molecular complex. In those simulations, the calculated $dt\mu$ -formation rates for 3-K gas targets (such as that shown in Fig. 11) were applied because the theoretical formation rates for a low-pressure solid were not available. A detailed analysis of the data was performed by Fujiwara [19]. He found more dt -fusion events at lowest and highest $t\mu$ energies than it was predicted using the perfect gas model. Much broader

resonance peaks, which we present in Fig. 10, can certainly improve the fits to the TRIUMF data. Also, the analysis of the fusion-product yield [19] proved that the low-energy $dt\mu$ -formation rate in solid deuterium was much higher than that predicted by the two-collision gas model. In particular, this concerns formation for the state $F = 1$. The theoretical rates presented in Fig. 9 support this finding.

A two-peak structure of the calculated time-of-flight spectra for $dt\mu$ resonances in HD, obtained assuming a 3-K gas model, was not confirmed by the solid-HD data [21]. However, one may expect much better agreement with the TRIUMF data when the rate shown in Fig. 12 is used instead of the very pronounced peaks evaluated for a 3-K HD gas. A possibility of wider resonance peaks with a fixed Doppler width of 50 meV was already considered in Ref. [21], which did not give good fits to the data. Such a result is now clear since, according to Eq. (53), the Doppler width of a resonance in a condensed target increases with the rising recoil energy ω_R . Simultaneously, the resonance height (59) decreases for higher ω_R so that the resonance strength is preserved.

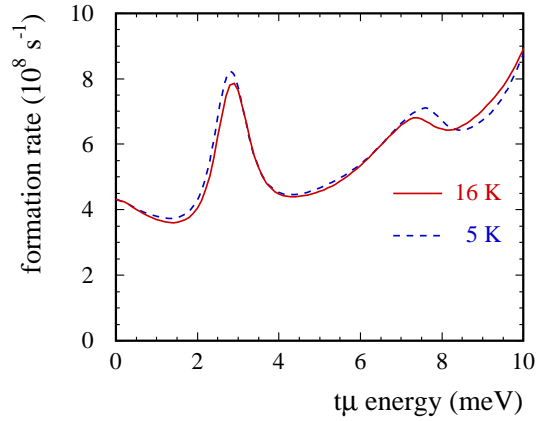


FIG. 14: Rate of resonant $dt\mu$ formation in $t\mu(F = 0)$ scattering from a D_2 molecule bound in 5-K and 16-K solid D/T($C_t = 0.4$) targets.

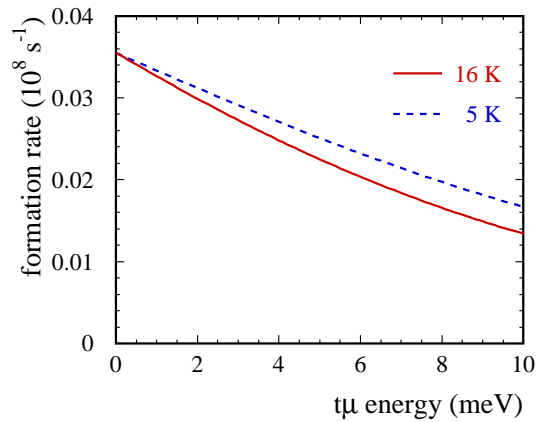


FIG. 15: Rate of resonant $dt\mu$ formation in $t\mu(F = 0)$ scattering from a DT molecule bound in 5-K and 16-K solid D/T($C_t = 0.4$) targets.

In Figs. 14 and 15 are shown the resonant-formation rates for the molecules D_2 and DT bound in a solid D/T target. An equilibrated mixture of the molecules D_2 , DT , and T_2 is assumed, for the tritium isotopic concentration $C_t = 0.4$. Target temperatures 5–16 K were applied in the RIKEN-RAL experiment, in which an unexpected temperature dependence of the $dt\mu$ -formation rate in solid D/T mixtures [18] was found. The corresponding target density is almost constant. A similar hydrogens mixture, kept at 15 K, was also used in the PSI experiment [4]. In the both experiments, time spectra of neutrons from dt fusion were measured. The data were interpreted using a standard steady-state kinetics, assuming that $t\mu$ atoms were thermalized. Formation from the state $F = 1$ is negligible for an appreciable tritium concentration as the spin-flip transition $F = 1 \rightarrow 0$ in low-energy $t\mu + t$ collision is very fast [50]. The theoretical energy-dependent $dt\mu$ -formation rates display a weak temperature dependence. One can expect such a behavior since, for any temperature of a low-pressure hydrogen-isotope solid, the limit $T/\Theta_D \ll 1$ is achieved ($\Theta_D \approx 100$ K) and changes of Θ_D are very small [27, 28]. As a result, the response function (69) and thus the formation rate (70) are always close to their limits for $T/\Theta_D \rightarrow 0$. Therefore, changes of the average formation rate, determined using steady-state conditions, can only be ascribed to different $t\mu$ -energy distributions corresponding to various target temperatures. An accurate comparison of the theory with data requires Monte Carlo simulations of the μCF cycle in a given solid D/T mixture, which can be performed in future after completion of a full set of the differential cross section for muonic atom scattering in mixed D/T crystals. The $t\mu$ -energy distribution in steady-state conditions is a crucial information. A shape of such a distribution is non-Maxwellian and the mean $t\mu$ energy is greater than $\frac{3}{2}k_B T$, due to solid-state effects and a possible admixture of epithermal $t\mu$'s from the reaction $d\mu + t \rightarrow t\mu + d$ and from back decay of the muonic-molecular complex. The latter effect was studied in Refs. [38, 51] with the use of Monte Carlo simulations, in the case of gas and liquid targets. In a high-density target with medium or high C_t , this effect is small, which is confirmed by the PSI fits [4].

Averaging the energy-dependent rate from Fig. 14 over the $t\mu$ -energy distribution leads to the mean resonant rate shown in Fig. 16. The energy distribution of $t\mu$ atoms, being

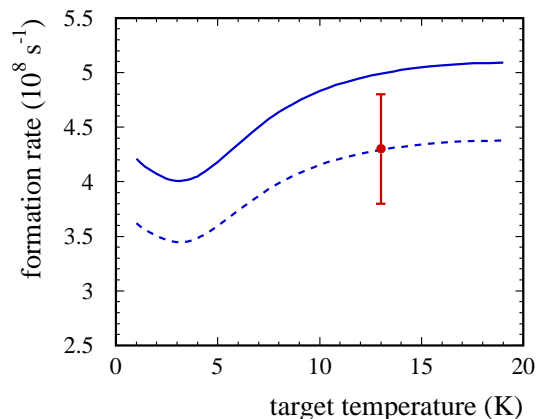


FIG. 16: Mean rate of resonant $dt\mu$ formation in $t\mu(F = 0)$ scattering from nD_2 molecules bound in solid D/T ($C_t = 0.4$) as a function of the target temperature. The dashed line represents the same rate scaled by the factor $S_\lambda = 0.86$. Also is shown the result of PSI measurement [4] for a similar target ($T = 13$ K, $\varphi = 1.45$).

in thermal equilibrium with phonons, is assumed to be proportional to $Z(\varepsilon) n_B(\varepsilon, T)$. The average $t\mu$ energy obtained using this function ranges from 1.2 meV for $T = 5$ K to 3.4 meV for $T = 16$ K. It is evident that the rise of the formation rate, above about 3 K, is mainly due to $t\mu$ entering into the region of the recoil-less resonant peak in para-D₂, centered at 2.7 meV. Phonon processes in both ortho-D₂ and para-D₂ lead to a smaller rise of the rate. The calculated formation rate is close to the PSI result for $T = 13$ K [4]. A coincidence of the theoretical curve with the data is obtained, as in the case of the TRIUMF measurements [20], on scaling by the factor $S_\lambda < 1$, which can be ascribed to inaccuracy of the calculated transition-matrix elements. Here, we have $S_\lambda = 0.86$, which is consistent with the result of Ref. [20].

In the RIKEN-RAL experiment [18], about 20% decrease of the μ CF effectiveness has been found for the target-temperature change from 16 to 5 K, independently of the tritium concentration. In order to explain this effect, several hypotheses have been considered. The hypothesis of a significant change of the mean resonant $dt\mu$ formation rate $\tilde{\lambda}_{dt\mu}^0$ (for $F = 0$) has led to best fits to the data. Kawamura et al assume that the two components of $\tilde{\lambda}_{dt\mu}^0$, namely the rate $\tilde{\lambda}_{dt\mu}^{0,D_2}$ of resonant formation for the D₂ molecule and the analogous rate $\tilde{\lambda}_{dt\mu}^{0,DT}$ for the DT molecule, are comparable. At 16 K, they use $\tilde{\lambda}_{dt\mu}^{0,D_2} = 3.5 \times 10^8 \text{ s}^{-1}$ and $\tilde{\lambda}_{dt\mu}^{0,DT} = 1.6 \times 10^8 \text{ s}^{-1}$ [18]. All temperature dependence of $\tilde{\lambda}_{dt\mu}^0 \equiv C_d \tilde{\lambda}_{dt\mu}^{0,D_2} + C_t \tilde{\lambda}_{dt\mu}^{0,DT}$ (C_d is the deuterium isotopic concentration) is ascribed only to $\tilde{\lambda}_{dt\mu}^{0,D_2}$. Other rates in the steady-state kinetics being fixed, about 30% decrease of $\tilde{\lambda}_{dt\mu}^{0,D_2}$ between 16 K and 5 K has been obtained. Thus, for $C_t = 0.4$, the respective change of $\tilde{\lambda}_{dt\mu}^0$ equals about 25%. This finding agrees quite well with analogous 20% decrease of the theoretical rate plotted in Fig. 16. However, theory predicts that the low-energy rate $\tilde{\lambda}_{dt\mu}^{0,DT}$ should be smaller by a few orders of magnitude than the corresponding rate $\tilde{\lambda}_{dt\mu}^{0,D_2}$, since the strong resonances in $t\mu$ +DT scattering are far from the region $\varepsilon \approx 0$. Averaging the rate presented in Fig. 15 over the $t\mu$ -energy distribution gives $\tilde{\lambda}_{dt\mu}^{0,DT} = 2.6 \times 10^6 \text{ s}^{-1}$. This value agrees well with the rate $\tilde{\lambda}_{dt\mu}^{0,DT} = (1.8 \pm 0.7) \times 10^6 \text{ s}^{-1}$, determined for a 30-K liquid D/T in the PSI experiment [4]. Note that the formation rate in the solid is somewhat greater than the corresponding rate in the liquid, which is a general law confirmed by experiments. Thus, according to the presented calculation and to the PSI results, $\tilde{\lambda}_{dt\mu}^0 \approx \tilde{\lambda}_{dt\mu}^{0,D_2}$. This means that in the steady-state analysis of Ref. [18], a somewhat greater value of $\tilde{\lambda}_{dt\mu}^{0,D_2}$ should have been assumed. In fact, Monte-Carlo simulations similar to that performed for gaseous D/T [38] are indispensable for an accurate analysis of such experiments, since several rates change significantly at lowest energies and thermalization process of muonic atoms in solid hydrogens is complicated [29, 52, 53]. It depends on the target temperature, isotopic concentration, and rotational population. A full set of the differential cross sections for muonic atom scattering in mixed solid D/T is necessary for accurate description of μ CF in such a target.

V. CONCLUSIONS

A method of calculating the rates of muonic-molecule resonant formation in collision of muonic atoms with condensed hydrogens has been developed. In the case of polycrystalline hydrogen-isotope targets, detailed calculations have been performed using the Debye model of an isotropic harmonic solid. Values of the resonant-formation rates have been computed for resonant $dt\mu$ formation in frozen D/T and HD targets, for collision energies $\lesssim 1$ eV.

These rates are very different from those obtained for dilute gaseous hydrogens and exhibit strong solid-state effects.

At lowest energies, contributions to the total rate from formation in a rigid lattice and from formation with simultaneous phonon processes can be distinguished. In the high-energy region ($\varepsilon \gtrsim 0.1$ eV), for any target, the rate takes a general asymptotic form, which depends on the mean kinetic energy of a target molecule. For low-pressure solid and liquid hydrogens, this energy is much greater than the corresponding energy in a perfect gas. As a result, condensed-matter effects in resonant formation do not disappear even at highest collision energies. Since the main $dt\mu$ resonances for HD and DT are located far from zero energy, in these cases it is sufficient to use only the asymptotic expression for the formation rate.

The calculated resonance profiles in solid are much broader than in the dilute-gas case. Experimental evidence supporting this conclusion has been found in the time-of-flight measurements of $dt\mu$ resonances at TRIUMF. A quantitative comparison of the theory with these experiments requires however complicated Monte-Carlo simulations.

The mean values of the $dt\mu$ -formation rates for D_2 bound in the solid D/T mixtures, averaged over the $t\mu$ kinetic energy under the steady-state conditions, agree well with the PSI and RIKEN-RAL data. Also a temperature dependence of the mean formation rate, determined at RIKEN-RAL for temperatures 5–16 K, is revealed by the theory.

Acknowledgments

We would like to thank Profs. K. Nagamine and L. I. Ponomarev for supporting this research and Drs. M. C. Fujiwara and G. M. Marshall for valuable discussions.

-
- [1] S. S. Gershtein and L. I. Ponomarev, Phys. Lett. B **72**, 80 (1977).
 - [2] S. E. Jones, A. N. Anderson, A. J. Caffrey, et al., Phys. Rev. Lett. **56**, 588 (1986).
 - [3] W. H. Breunlich, M. Cargnelli, P. Kammel, et al., Phys. Rev. Lett. **58**, 329 (1987).
 - [4] P. Ackerbauer, J. Werner, W. H. Breunlich, et al., Nucl. Phys. A **652**, 311 (1999).
 - [5] W. H. Breunlich, P. Kammel, J. S. Cohen, and M. Leon, Ann. Rev. Nucl. Part. Sci. **39**, 311 (1989).
 - [6] L. I. Ponomarev, Contemp. Phys. **31**, 219 (1990).
 - [7] P. Froelich, Adv. Phys. **41**, 405 (1992).
 - [8] E. A. Vesman, Pis'ma Zh. Eksp. Teor. Fiz. **5**, 113 (1967), [JETP Letters **5**, 91 (1967)].
 - [9] Yu. V. Petrov, Phys. Lett. B **163**, 28 (1985).
 - [10] L. I. Menshikov and L. I. Ponomarev, Phys. Lett. B **167**, 141 (1986).
 - [11] L. I. Menshikov, Fiz. Elem. Chastits At. Yadra **19**, 1349 (1988), [Sov. J. Part. Nucl. **19**, 583 (1988)].
 - [12] J. S. Cohen and M. Leon, Phys. Rev. A **39**, 946 (1989).
 - [13] M. P. Faifman, L. I. Menshikov, and T. A. Strizh, Muon Catal. Fusion **4**, 1 (1989).
 - [14] M. P. Faifman and L. I. Ponomarev, Phys. Lett. B **265**, 201 (1991).
 - [15] M. Leon, Phys. Rev. A **49**, 4438 (1994).
 - [16] Yu. V. Petrov and V. Yu. Petrov, Phys. Lett. B **378**, 1 (1996).
 - [17] Y. Averin, V. R. Bom, A. M. Demin, et al., Hyp. Interact. **138**, 249 (2001).

- [18] N. Kawamura, K. Nagamine, T. Matsuzaki, et al., Phys. Rev. Lett. **90**, 043401 (2003).
- [19] M. C. Fujiwara, Ph.D. thesis, University of British Columbia (1999).
- [20] M. C. Fujiwara, A. Adamczak, J. M. Bailey, et al., Phys. Rev. Lett. **85**, 1642 (2000).
- [21] T. A. Porcelli, A. Adamczak, J. M. Bailey, et al., Phys. Rev. Lett. **86**, 3763 (2001).
- [22] G. M. Marshall, A. Adamczak, J. M. Bailey, et al., Hyp. Interact. **138**, 203 (2001).
- [23] W. E. Lamb, Phys. Rev. **55**, 190 (1939).
- [24] K. S. Singwi and A. Sjölander, Phys. Rev. **120**, 1093 (1960).
- [25] L. Van Hove, Phys. Rev. **95**, 249 (1954).
- [26] K. Fukushima, Phys. Rev. A **48**, 4130 (1993).
- [27] I. F. Silvera, Rev. Mod. Phys. **52**, 393 (1980), and references therein.
- [28] P. C. Souers, *Hydrogen Properties for Fusion Energy* (University of California Press, Berkeley, 1986).
- [29] A. Adamczak and M. P. Faifman, Phys. Rev. A **64**, 052705 (2001).
- [30] P. E. Knowles, G. A. Beer, G. R. Mason, et al., Phys. Rev. A **56**, 1970 (1997).
- [31] L. I. Menshikov, Muon Catal. Fusion **2**, 273 (1988).
- [32] V. N. Ostrovski and V. I. Ustimov, Zh. Eksp. Teor. Fiz. **79**, 1228 (1980), [Sov. Phys. JETP **52**, 620 (1980)].
- [33] N. T. Padial, J. S. Cohen, and R. B. Walker, Phys. Rev. A **37**, 329 (1988).
- [34] U. Fano, Phys. Rev. **124**, 1866 (1961).
- [35] C. Petitjean, D. V. Balin, W. H. Breunlich, et al., Hyp. Interact. **118**, 127 (1999).
- [36] C. Petitjean, Hyp. Interact. **138**, 191 (2001).
- [37] S. E. Jones, S. E. Anderson, A. J. Caffrey, et al., Phys. Rev. Lett. **51**, 1757 (1983).
- [38] M. Jeitler, W. H. Breunlich, M. Cargnelli, et al., Phys. Rev. A **51**, 2881 (1995).
- [39] Yu. V. Petrov and V. Yu. Petrov, Zh. Eksp. Teor. Fiz. **100**, 56 (1991), [Sov. Phys. JETP **73**, 29 (1991)].
- [40] Yu. V. Petrov, V. Yu. Petrov, and H. H. Schmidt, Phys. Lett. B **331**, 266 (1994).
- [41] A. Akhiezer and I. Pomeranchuk, Zh. Eksp. Teor. Fiz. **17**, 769 (1947), [Sov. Phys. JETP **11**, 167 (1947)].
- [42] G. C. Wick, Phys. Rev. **94**, 1228 (1954).
- [43] S. W. Lovesey, *Theory of Neutron Scattering from Condensed Matter* (Clarendon Press, Oxford, 1984).
- [44] B. D. Josephson, Phys. Rev. Lett. **4**, 341 (1960).
- [45] F. J. Mompeán, M. Garcia-Hernández, F. J. Bermejo, and S. M. Bennington, Phys. Rev. B **54**, 970 (1996).
- [46] H. Bethe and G. Placzek, Phys. Rev. **51**, 450 (1937).
- [47] M. P. Faifman, T. A. Strizh, E. A. G. Armour, and M. R. Harston, Hyp. Interact. **101/102**, 179 (1996).
- [48] A. Toyoda, K. Ishida, K. Shimomura, et al., Phys. Rev. Lett. **90**, 243401 (2003).
- [49] T. M. Huber, A. Adamczak, J. M. Bailey, et al., Hyp. Interact. **118**, 159 (1999).
- [50] A. Adamczak, M. P. Faifman, L. I. Ponomarev, et al., Atomic Data and Nuclear Data Tables **62**, 255 (1996).
- [51] J. S. Cohen, Phys. Rev. A **34**, 2719 (1986).
- [52] A. Adamczak, Hyp. Interact. **119**, 23 (1999).
- [53] J. Woźniak, A. Adamczak, G. A. Beer, et al., Phys. Rev. A **68**, 062502 (2003).